

Multidimensional dissipative solitons and solitary vortices

B. A. Malomed

Department of Physical Electronics, School of Electrical Engineering,

Faculty of Engineering, Tel Aviv University, Tel Aviv 69978, Israel

Instituto de Alta Investigación, Universidad de Tarapacá, Casilla 7D, Arica, Chile

This article offers a review of (chiefly, theoretical) results for self-trapped states (solitons) in two- and three-dimensional (2D and 3D) models of nonlinear dissipative media. The existence of such solitons requires to maintain two stable balances: between nonlinear self-focusing and linear spreading (diffraction and/or dispersion) of the physical fields, and between losses and gain in the medium. Due to the interplay of these conditions, dissipative solitons exist, unlike solitons in conservative models, not in continuous families, but as isolated solutions (*attractors*). The main issue in the theory is stability of multidimensional dissipative solitons, especially ones with *embedded vorticity*. First, stable 2D dissipative solitons are presented in the framework of the complex Ginzburg-Landau equation with the cubic-quintic nonlinearity, which combines linear loss, cubic gain, and quintic loss (the linear loss is necessary to stabilize zero background around dissipative solitons, while the quintic loss provided for the global stability of the setting). In addition to fundamental (zero-vorticity) solitons, stable *spiral solitons* produced by the CGL equation are produced too, with intrinsic vorticities $S = 1$ and 2 . Stable 2D solitons were also found in a system built of two linearly-coupled optical fields, with linear gain acting in one and linear loss, which plays the stabilizing role, in the other. In this case, the inclusion of the cubic loss (without quintic terms) is sufficient for the creation of stable fundamental and vortical dissipative solitons in the linearly-coupled system. In addition to truly localized states, weakly localized ones are presented too, in the single-component model with nonlinear losses, which does not include explicit gain. In that case, the losses are compensated by the influx of power from the reservoir provided, at the spatial infinity, by the weakly localized structure of the solution. Other classes of 2D models which are considered in this review make use of spatially modulated loss or gain to predict many species of robust dissipative solitons, including localized dynamical states featuring complex periodically recurring metamorphoses. Stable fundamental and vortical solitons are also produced by models including a trapping or spatially periodic potential. In the latter case, the consideration addresses 2D *gap dissipative solitons* as well. 2D two-component dissipative models including spin-orbit coupling are considered too. They give rise to stable states in the form of *semi-vortex* solitons, with vorticity carried by one component. In addition to the 2D solitons, the review includes 3D fundamental and vortical dissipative solitons, stabilized by the cubic-quintic nonlinearity and/or external potentials. Collisions between 3D dissipative solitons are considered too.

Contents

I. Introduction	2
II. Spiral solitons (vortex rings) produced by the 2D complex Ginzburg-Landau (CGL) equation with the cubic-quintic (CQ) nonlinearity	3
III. Dissipative vortex solitons in a laser cavity stabilized by the linearly coupled lossy feedback	7
IV. Weakly localized modes in media with nonlinear losses (multi-photon absorption)	9
V. Localized states in 2D nonlinear dissipative media with spatially modulated gain or loss	10
A. Vortex solitons supported by the 2D cubic-quintic CGL equations with spatially modulated linear losses	11
B. Complex modes supported by the 2D cubic-quintic CGL equation with localized linear gain	12
C. Stable vortices supported by the cubic CGL equation with localized gain applied along a ring	14
VI. Two-dimensional DSs (dissipative solitons) in the HO (harmonic-oscillator) trapping potential	15
A. The CGL equation with the CQ nonlinearity and linear loss	15
B. The cubic CGL equation with linear gain	17

VII. Dissipative vortex solitons stabilized by spatially periodic (lattice) potentials	18
A. Crater-shaped (tightly confined) vortex solitons	18
B. Multi-peak vortex solitons	19
C. Dissipative gap solitons (GSs) generated by the CGL equation with the 2D lattice potential	21
VIII. Two-component dissipative solitons of the vortex-antivortex (VAV) type stabilized by SOC (spin-orbit coupling)	24
A. The model	24
B. Results	26
IX. Three-dimensional dissipative solitons	27
A. 3D solitons in the free space	27
B. Collisions between 3D vortex solitons	28
C. Quasi-stable 3D vortex solitons supported by 2D potential lattices or a trapping potential	35
X. Conclusion	35
Acknowledgments	37
References	37

Acronyms

1D – one-dimensional
2D – two-dimensional
3D – three-dimensional
BEC – Bose-Einstein condensate
b.c. – boundary conditions
CGL – complex Ginzburg-Landau (equation)
CSV – crater-shaped vortex
CQ – cubic-quintic (nonlinearity)
DS – dissipative soliton
FT – flat-top (shape of a broad soliton)
GS – gap soliton
GVD – group-velocity dispersion
HO – harmonic-oscillator (trapping potential))
IS – intersite (centered mode)
LL – Lugiato - Lefever (equation)
NLS – nonlinear-Schrödinger (equation)
OS – onsite (centered modes)
\mathcal{PT} – parity-time (symmetry)
SV – semi-vortex
VR – vortex ring

I. INTRODUCTION

Studies of pattern formation in nonlinear media combining conservative and dissipative properties is a vast research area with many physical realizations [1–3]. A broad class of universal models for the pattern formation in many physical settings is provided by complex Ginzburg-Landau (CGL) equations [4, 5]. In many cases, especially as concerns nonlinear optics, CGL equations are consistently derived from the underlying physical theory; in some other cases, the same equations are introduced as useful phenomenological models.

Many patterns which were predicted theoretically and created experimentally in nonlinear dissipative media exhibit a trend to self-trapping into localized states, alias dissipative solitons (DSs), which are important physical objects in many areas of physics, especially in nonlinear photonics and optics [6–12]. In most cases, DSs are adequately represented by diverse localized solutions of CGL equations. The theory of DSs was developed in detail in one-dimensional (1D) settings, starting from the famous, although unstable, Pereira-Stenflo solitons [13, 14], which are exact solutions of the 1D CGL equation with the cubic nonlinearity. Essentially more challenging are studies of DSs in two- and three-dimensional (2D and 3D) geometries. A highly promising peculiarity of multidimensional solitons is a possibility to embed vorticity into them, thus making such solitons self-trapped states with an intrinsic topological structure [15]. On the other hand, it is well known that multidimensional solitons are often subject to instabilities,

therefore a problem of cardinal significance is to develop physically relevant models which admit the creation of stable 2D and 3D solitons, especially those with internal structure, such as localized modes with embedded vorticity [16]-[20].

The objective of this article is to produce a sufficiently systematic review of results (chiefly, theoretical ones) produced by the work in the vast area of studies of multidimensional DSs. The review includes both relatively old models elaborated in this area and more recent ones, along with basic findings obtained by the studies of these models. The main topics addressed in the article correspond to sections in the article's table of contents. They are determined, primarily, by mechanisms providing stabilization of DSs, both fundamental (zero-vorticity) and internally-structured (in particular, vorticity-carrying) ones, in 2D and 3D settings. The basic DS-stabilization mechanisms, elaborated in many theoretical and some experimental works, which are presented in the current review, can be summarized as follows.

(i) The use of the CGL equations with combinations of competing nonlinear terms. In most cases, these are cubic and quintic (CQ) ones, in both conservative and dissipative parts of the equations. In the framework of such models, which, in particular, describe lasing optical setups with saturable absorption, the gain is provided by the cubic term, while a lossy quintic one must be included to secure the global stability of the system against the blowup [21]. This mechanism dominates in the 2D and 3D settings, which are considered, respectively, in Sections II and IX of the article. A related mechanism, based on nonlinear absorption, plays the dominant role in the stabilization of weakly localized nonlinear dissipative modes, both fundamental and vortical ones, which are considered in Section IV.

(ii) Stabilization of 2D DSs in a laser cavity with the linear gain and cubic nonlinearity by means of a lossy feedback, which is linearly coupled to the cavity. This system is considered in Section III.

(iii) Stabilization of 2D DSs, many of which exhibit complex intrinsic structure and dynamics, by means of spatially modulated gain and/or loss. This class of the models and DSs produced by them is the subject of Section V.

(iv) Stabilization of 2D (Sections VI and VII) and 3D (Section IX) DSs with the help of trapping potentials, which may be represented by harmonic-oscillator (HO) or spatially-periodic (lattice) potential terms in the respective CGL equations.

(v) Stabilization of 2D two-component DSs, built as vortex-antivortex (VAV) bound states by means of the spin-orbit coupling (SOC), is the subject of Section VIII.

These topics, which are included, in a sufficiently detailed form, in the present review cover only a part of results accumulated in the work performed in the vast area of DSs. The choice of this set of the topics is suggested, in particular, by research interests of the author. A really comprehensive review of the theoretical and experimental work with DSs and related objects should be a subject of a full-size book, rather than of a single article. Some essential topics which are not considered in the review are mentioned in the concluding section.

II. SPIRAL SOLITONS (VORTEX RINGS) PRODUCED BY THE 2D COMPLEX GINZBURG-LANDAU (CGL) EQUATION WITH THE CUBIC-QUINTIC (CQ) NONLINEARITY

In its simplest form, the CGL equation with the cubic nonlinearity, for 2D complex field $U(x, y)$, may be considered as the generalization of the corresponding cubic nonlinear Schrödinger (NLS) equation with complex coefficients:

$$\frac{\partial U}{\partial z} = \delta U + \left(\beta + \frac{i}{2} \right) \left(\frac{\partial^2}{\partial x^2} + \frac{\partial^2}{\partial y^2} \right) U - (\varepsilon - ig) |U|^2 U. \quad (1)$$

This equation is written in terms of the light propagation in bulk media, with propagation distance z and transverse coordinates (x, y) [2, 22]. In Eq. (1) term $(i/2)(U_{xx} + U_{yy})$ represents the paraxial diffraction, $g > 0$ is the coefficient of the cubic (Kerr) self-focusing (or cubic defocusing, in the case of $g < 0$), while coefficients $\beta > 0$ and $\varepsilon > 0$ account for, respectively, the linear dispersive losses (alias diffusion, or viscosity, in terms of hydrodynamics) and the cubic loss (two-photon absorption, in terms of optics). Finally, coefficient $\delta > 0$ represents linear gain, which is necessary for the compensation of the dispersive and nonlinear losses.

The cubic CGL equation (1) is not an appropriate model for predicting robust localized states, such as DSs, because the presence of the term with $\delta > 0$ destabilizes the zero solution against small perturbations, hence the zero background around localized states is unstable, making such states unstable as a whole too. To introduce a model which admits stable DSs, one needs to replace the linear loss by gain in Eq. (1), i.e., reverse the sign of δ . Simultaneously, the sign of the cubic dissipative coefficient must be reversed too, $\varepsilon \rightarrow -\varepsilon$, so that the cubic term provides for *nonlinear gain*. Finally, to prevent the blowup of the system, it is necessary to add a quintic loss term, with some coefficient $\mu > 0$, which turns the 2D CGL equation into one of the CQ type, as first proposed by Sergeev and Petviashvili in 1984 [23]:

$$\left(\frac{\partial}{\partial z} + \delta \right) U = \left(\beta + \frac{i}{2} \right) \left(\frac{\partial^2}{\partial x^2} + \frac{\partial^2}{\partial y^2} \right) U + (\varepsilon + i\sigma) |U|^2 U - (\mu + i\nu) |U|^4 U. \quad (2)$$

In this equation, necessary signs of the coefficients are

$$\delta > 0, \beta \geq 0, \varepsilon > 0, \mu > 0. \quad (3)$$

The scaling freedom makes it possible to fix $|\sigma| = 1$ in Eq. (2), while signs $\sigma = +1$ and $\sigma = -1$ correspond, respectively, to the self-focusing and defocusing cubic nonlinearity. Further, because Eq. (2) includes the quintic dissipative term with coefficient μ , it is also natural to introduce the quintic correction to the cubic self-interaction, with coefficient ν in Eq. (2). Usually, it is assumed that this quintic terms represents self-defocusing, which corresponds to $\nu > 0$ in Eq. (3), as quintic self-focusing in the 2D geometry leads to the supercritical collapse [24–26]. Nevertheless, in the presence of the quintic loss, the quintic self-interaction may have the focusing sign too ($\nu < 0$), as the quintic loss arrests the collapse in that case [27–29].

While the CQ combination of the nonlinear dissipation and gain was originally postulated phenomenologically [23], this pair of terms provides an appropriate model of nonlinear amplifiers in optics, which are built as a juxtaposition of the usual saturable amplifier (featuring the linear gain in a combination with cubic and quintic losses) and saturable absorber [30–32, 34]. Such setups are very efficient for the generation of stable temporal solitons in fiber lasers [33]. The two-dimensional CGL equation with the CQ nonlinearity was derived as a dynamical model for coupled arrays of lasers by [35].

Stationary solutions to Eq. (2), which carry a real propagation constant k and integer vorticity S , are looked for in the usual form, written in polar coordinates (r, θ) (instead of the Cartesian coordinates (x, y)),

$$U(r, \theta, z) = A(r) \exp(ikz + iS\theta), \quad (4)$$

with amplitude function $A(r)$ determined by the radial equation, obtained from the substitution of ansatz (4) in CGL equation (2):

$$(ik + \delta) A = \left(\beta + \frac{i}{2} \right) \left(\frac{d^2}{dr^2} + \frac{1}{r} \frac{d}{dr} - \frac{S^2}{r^2} \right) A + (\varepsilon + ig) |A|^2 A - (\mu + i\nu) |A|^4. \quad (5)$$

DS solution $A(r)$ of Eq. (5) is a complex function, while in the conservative model, with $\delta = \beta = g = \nu = 0$, relevant solutions, including vortex-ring (VR) ones, take a real form. A principal difference from the conservative counterpart is that DS solutions exist at isolated values of k , while solitons in conservative models (as well as in parity-time (\mathcal{PT})-symmetric ones, which include spatially separated mutually-balanced linear-gain and loss terms, lying at the border between conservative and dissipative systems [36, 38]), form continuous families, parameterized by propagation constant k , that takes values in certain intervals populated by the solitons (most typically, it is the semi-infinite bandgap). This difference is explained by the fact that, in addition to the balance between the nonlinear self-focusing and diffractive expansion, which is necessary for the existence of any soliton in conservative models, DSs must satisfy the additional constraint, *viz.*, the balance between the gain and losses. It is also relevant to mention 2D localized states in the form of “chiral bubbles”, which are produced by the CQ CGL equation with real coefficients, and additional chiral terms. Such states were experimentally observed in nematic liquid crystals [37].

Basic result for the existence and stability of localized solutions of Eqs. (2) and (5) with $S = 0, 1$, and 2 were reported in Ref. [39]. In most cases, direct simulations of Eq. (2) demonstrate that an input with winding number S (introduced as in Eq. (4)) and a radial shape which decays at $r \rightarrow \infty$ and, in the case of $S \geq 1$, vanishes $\sim r^S$ at $r \rightarrow 0$ (or remains finite at $r = 0$ in the case of $S = 0$), quickly transforms into a stable VR, as shown in Fig. 1.

Radial profiles of the stable solitons produced in Fig. 1, along with their fundamental-vortex counterpart with $S = 0$, are displayed in Fig. 2. Further, for the same VRs with $S = 1$ and 2 top views of the spatial distribution of the amplitude, $|A(r)|$, and phase, which is defined, according to Eq. (4), as

$$\phi(r, \theta) = S\theta + \arg(A(r)), \quad (6)$$

are plotted in Fig. 3. Note that, due to the presence of the r -dependent term in Eq. (6), constant-phase lines, $\phi(r, \theta) = \text{const}$, in Fig. 3 are not circumferences, which they are in VR solutions of the NLS equation with real coefficients, but *spirals*, therefore the respective VR solutions are categorized as *spiral solitons*.

The results produced by the systematic numerical analysis if Eq. (5) are summarized by means of the plots displayed in Fig. 4. Because most important control parameters in this model are the coefficients of the cubic gain and quintic loss, *i.e.*, ε and μ , respectively, and the main characteristic of the 2D solitons is, as usual, their total norm (or power, in terms of the realization of the model in optics),

$$P = 2\pi \int_0^\infty |A(r)|^2 r dr, \quad (7)$$

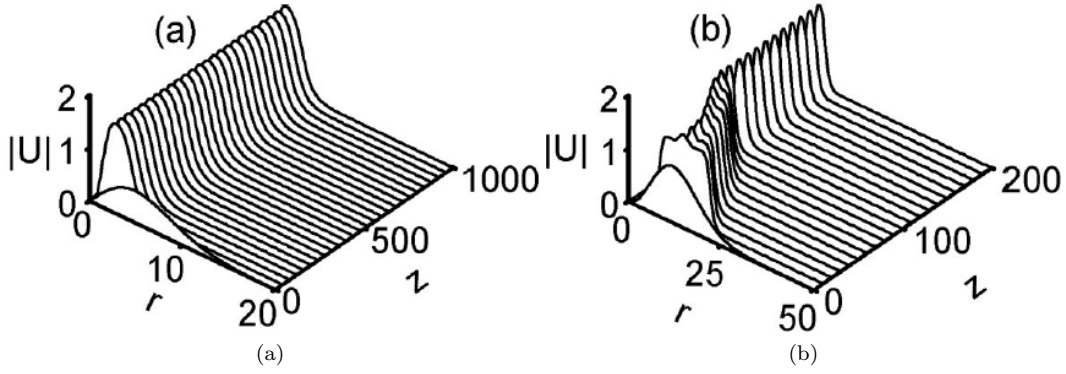


FIG. 1: Formation of spiral solitons with winding numbers $S = 1$ (a) and $S = 2$ (b), as produced by simulations of Eq. (2) with parameters $\delta = 0.5$, $\beta = 0.5$, $\varepsilon = 2.5$, $\nu = 0.1$, $\mu = 1$, and $\sigma = +1$. The input is taken as per Eq. (3) with the initial amplitude function $A_0(r) = 0.2r \exp(-(r/7)^2)$ in (a), and $A_0(r) = 0.02r^2 \exp(-(r/12)^2)$ in (b) (source: Ref. [39]).

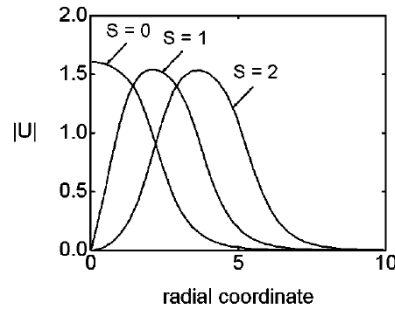


FIG. 2: Radial profiles of the stable spiral dissipative solitons with $S = 1$ and 2, whose formation is demonstrated in Fig. 1, and the same for the fundamental soliton, with $S = 0$ (source: Ref. [39]).

three families of stable DSs, with winding numbers $S = 0, 1$, and 2, are presented by means of curves $P(\mu)$ in Fig. 4(a) for fixed typical values of other parameters. Most essential results are displayed in Fig. 4(b) by means of the stability chart in parameter plane (μ, ε) . The stability was verified by means of direct simulations of the perturbed evolution of the solitons, as well as through computation of stability eigenvalues for small perturbations around the stationary soliton solutions [39]. As seen in Fig. 4(b), the stability area expands with the increase of μ and ε , and multistability, i.e., coexistence of the stable solitons with different values of S is a noteworthy feature of the model.

An essential peculiarity of spiral solitons produced by the two-dimensional CGL equation (2), with $S \geq 1$, is that they are *completely unstable* against spontaneous splitting in the absence of the dispersive losses (diffusion), $\beta = 0$,

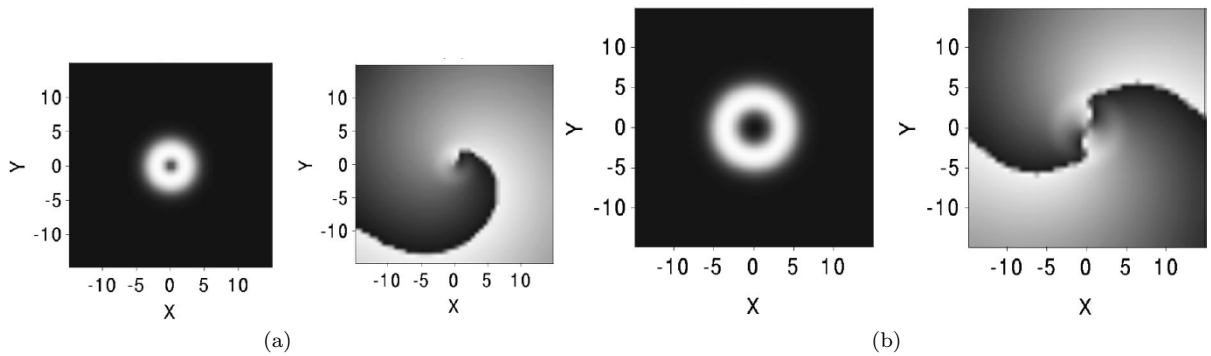


FIG. 3: Top views of the amplitude, $|A(r)|$, and phase, defined as per Eq. (6), of the same stable spiral solitons with $S = 1$ and 2 (left and right pairs of panels, respectively) which are presented in Figs. 1 and 2 (source: Ref. [39]).

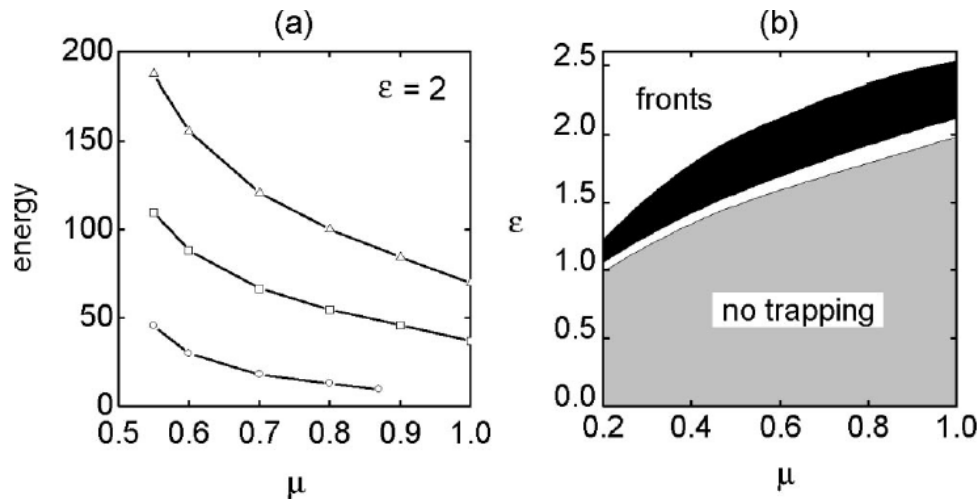


FIG. 4: (a) The total power of the stable two-dimensional DSs, defined as per Eq. (7) (here called “energy”) vs. the quintic loss coefficient μ for a fixed value of the cubic-gain coefficient in Eq. (2), $\varepsilon = 2.5$. Other parameters are $\delta = \beta = 0.5$, $\nu = 0.1$, and $\sigma = +1$. Chains of circles, squares, and triangles represent, respectively, the DSs with winding numbers $S = 0, 1$, and 2 . (b) The existence domain in the parameter plane (μ, ε) for the same stable solitons, and the same values of δ, β , and ν as in panel (a). In the black region of full multistability, the stable solitons with $S = 1, 2$, and 3 coexist. The narrow lower white strip is a bistability area, in which they exist stable spiral solitons with $S = 1$ and 2 , while the fundamental ones, with $S = 0$, are absent. No stable solitons exist in the gray region (“no trapping”). In the upper white region, localized inputs do not self-trap into solitons, but rather expand in the radial direction in the form of “fronts” (source: [39]).

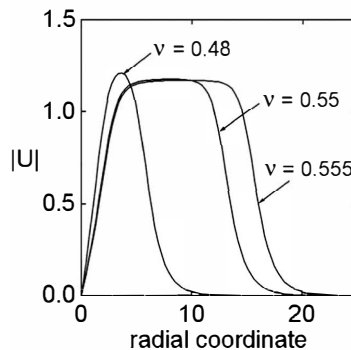


FIG. 5: The transition from the narrow stable VR radial profile (for $S = 1$) to a broad FT one with the variation of the quintic self-defocusing coefficient ν in Eq. (2), while other coefficients are fixed as $\varepsilon = 0.3$, $\delta = 0.05$, $\beta = 0.03$, $\mu = 0.2$, and $\sigma = +1$ (source: Ref. [46]).

while the fundamental DSs, with $S = 0$, may be stable in this case. Indeed, all the stable spiral solitons presented in Figs. 1 – 4 were obtained as solutions of Eq. (2) with $\beta > 0$. The instability of the spiral solitons in the case of $\beta = 0$ is an essential problem, because natural models of laser cavities, which are an essential source of CGL equations, do not include the diffusion term, for the reason that light propagates by rays, but not by diffusion (nevertheless, a diffusion term may appear in an effective CGL model derived from the system of Maxwell-Bloch equations, as shown by [40]). It is shown below, in Section V, that, in the absence of the diffusion term, VR modes may be stabilized by the HO potential added to the CGL equation [41], or, as shown in Section VI, by a spatially periodic potential [42]. Another possibility to stabilize localized vortex modes, outlined below in Section IV, is provided by spatial modulation of the local loss or gain [43–45].

A well-known feature of conservative NLS equation with the CQ nonlinearity is that the competition of the cubic self-focusing and quintic defocusing gives rise to the characteristic flat-top (FT) shape of stable 1D and 2D solitons. The fundamental and spiral solitons produced by the CGL equation (2) share this feature: FT profiles are generated by Eq. (2) close to the boundary between localized and delocalized states, as shown in Fig. 5.

Stable VR solutions with higher values of the winding number, up to $S = 20$, were found by means of numerical solutions of Eq. (2), in combination with some results produced by the variational approximation based on the complex

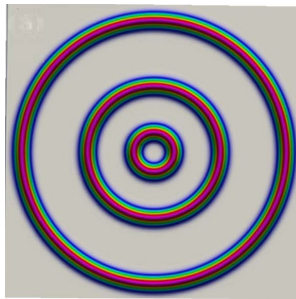


FIG. 6: An example of a stable nested multi-ring state produced by the numerical solution of Eq. (2): an inner VR with $S = 3$ embedded into the middle one with $S = 10$, which is embedded into the outer VR with $S = 20$ (source: Ref. [47]).

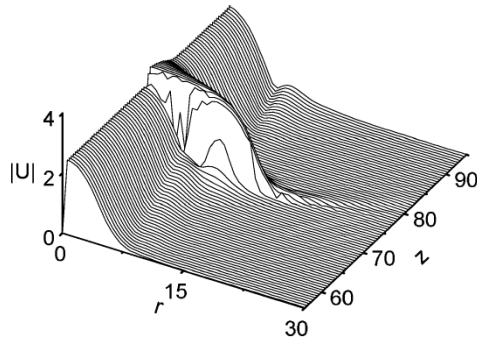


FIG. 7: An example of a sudden burst in the VR with $S = 1$, revealed by simulations of Eq. (2) with $\delta = \beta = 0.05$, $\varepsilon = 1.75$, $\mu = 0.2$, $\nu = 1.4$, and $\sigma = +1$. The long-time evolution exhibits a chain of bursts at random moments of time (source: [46]).

Lagrangian formally corresponding to Eq. (2) [47]. The same work reported the existence of stable concentric multi-ring states. In particular, there are solutions in which inner rings carry VRs with smaller values of S , which are surrounded by very broad rings carrying much larger S , see an example in Fig. 6. Dynamics of complex multi-vortex patterns was addressed by means of simulations of Eq. (2) in Ref. [48].

At parameter values where stationary spiral-vortex solutions of Eq. (2) are unstable, simulations demonstrate a possibility of robust nonstationary states. Most typical among them are periodically oscillating breathers, which were found, e.g., at $\delta = \beta = 0.05$, $\varepsilon = 0.3$, $\mu = 0.2$, $\nu = 2$, and $\sigma = +1$ [39]. A remarkable dynamical state is an *erupting* one, in the form of a randomly recurring sudden bursts of the quasi-stationary soliton, as shown in Fig. 7 (such solutions are similar to erupting states found in the 1D CGL equation [49]). An example of the burst is displayed in Fig. 6.

A special case of the CGL equation is one without dispersive losses, i.e., with $\beta = 0$ in Eq. (2) (recall that, in this case, only fundamental DSs may be stable, while all VRs are subject to splitting instability). This form of the CGL equation keeps the property of the Galilean invariance, hence a stable fundamental DS can be set in motion with an arbitrary speed by means of the Galilean boost. In turn, this possibility makes it possible to explore collisions between moving DSs. Simulations of the collisions between them demonstrate that, depending on parameters, the collisions may be quasi-elastic (the solitons separate after the collision, although with essentially different speeds), inelastic, with the two solitons merging into a single one, and destructive, leading to complete decay of the solitons triggered by the collision [50].

III. DISSIPATIVE VORTEX SOLITONS IN A LASER CAVITY STABILIZED BY THE LINEARLY COUPLED LOSSY FEEDBACK

As said above, the necessity to maintain stable zero background around the DS suggests to keep linear loss, $\delta > 0$, in the CGL equation (2). Then, the cubic gain, $\varepsilon > 0$, is necessary to compensate the loss, and the quintic loss, $\mu > 0$, must be added to prevent the blowup. Nevertheless, a system of linearly coupled equations of the CGL type, which admits the existence of stable DSs in the presence of the usual cubic dissipation (without “exotic” quintic terms) was introduced (originally, in the 1D form) in Ref. [51]. The original 1D system governs the copropagation of amplitudes $u(z, \tau)$ and $v(z, \tau)$ of optical waves in a dual-core fiber, with inter-core linear-coupling coefficient κ . In this setup, one

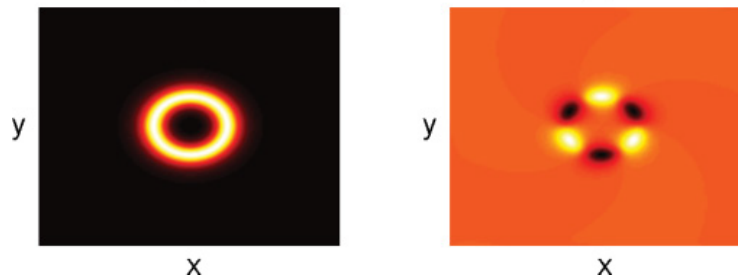


FIG. 8: Spatial profiles of the absolute value (a) and snapshot of the real part (b) of field $E(x, y)$ for a stable DS with embedded vorticity $S = 3$, which is produced by numerical solution of the system of coupled CGL equations (11) and (12). See further details in Ref. [54].

(“active”) core carries linear gain, accounted for by coefficient $\gamma_0 > 0$, while the other (“passive”) core is dissipative, with loss coefficient $\Gamma_0 > 0$. The corresponding CGL system is

$$iu_z + \left(\frac{1}{2} - i\gamma_1\right) u_{\tau\tau} + (1 + i\gamma_2)|u|^2u - i\gamma_0u + \kappa v = 0, \quad (8)$$

$$iv_z + \left(\frac{1}{2} - i\gamma_1\right) v_{\tau\tau} + |v|^2v + i\Gamma_0v + \kappa u = 0. \quad (9)$$

Here, z and $\tau \equiv t - z/V_{\text{gr}}$ are, as usual, the propagation distance and reduced time, with group velocity V_{gr} of the carrier wave [22], the anomalous-group-velocity-dispersion (GVD) and Kerr coefficients are scaled to be 1, while $\gamma_1 \geq 0$ and $\gamma_2 > 0$ account for the dispersive and nonlinear losses, respectively. Possible phase- and group-velocity mismatch between the two cores is not included in Eqs. (8) and (9), but its effect was studied too, see a review of the DS dynamics in 1D systems of this type in Ref. [52]. The competition of the linear gain and loss in the two cores of the system keeps stability of the zero solution if the linear-loss coefficient takes values in interval

$$\gamma_0 < \Gamma_0 < \kappa^2/\gamma_0 \quad (10)$$

(note that the dispersive-loss coefficient γ_1 does not appear in Eq. (10)). It was demonstrated by means of an analytical perturbation theory, that may be applied in the case of small coefficients $\gamma_{0,1,2}$ and Γ_0 [51], and in a general form by means of a numerical solution [53], that condition (10) is compatible with the existence of a pair of DSs produced by Eqs. (8) and (9), one of which (a higher-amplitude narrow one) is stable, while a lower-amplitude broad DS is unstable (it plays the role of a separatrix between attraction basins of the stable zero solution and stable DS).

The system of the linearly-coupled CGL equations with the cubic-only nonlinearity was extended into a 2D form and applied to construct stable two-dimensional DSs, including vortical ones [54]. The so defined 2D system is

$$\frac{\partial E}{\partial t} = (d + iD) \left(\frac{\partial^2}{\partial x^2} + \frac{\partial^2}{\partial y^2} \right) E + g_0E + g_2|E|^2E + F, \quad (11)$$

$$\frac{\partial F}{\partial t} = -\lambda F + \sigma E. \quad (12)$$

This model governs the time evolution of the optical-field amplitude E in a laser cavity of the VCSEL type with paraxial diffraction in the plane (x, y) , F being the feedback field generated by an external reflector. Real coefficients g_0 , λ , σ , d and the real part of the complex one g_2 are counterparts of constants γ_0 , Γ_0 , κ^2 , γ_1 and γ_2 in Eqs. (8) and (9). Unlike Eq. (9), the passive component of the present system, given by Eq. (12), does not include the diffraction and cubic nonlinearity, as these are not essential ingredients of the setup.

Numerical solution of Eqs. (11) and (12) readily create stable two-dimensional DSs with embedded vorticity $S = 0, 1, 2, 3, \dots$. An example is presented in Fig. 8. Additional results demonstrate that, for fixed parameters of Eqs. (11) and (12), the radius of stable VRs produced by these equations grows linearly with S [54].

A similar 2D system, with saturable nonlinearity instead of the cubic term, was considered in Ref. [55]. In that case too, stable vortex DSs were produced by a numerical solution of the system.

IV. WEAKLY LOCALIZED MODES IN MEDIA WITH NONLINEAR LOSSES (MULTI-PHOTON ABSORPTION)

Specific quasi-soliton states are generated by the NLS equation which includes higher-order nonlinear loss:

$$U_z = i(U_{xx} + U_{yy}) + i\alpha|U|^2U - |U|^{2M-2}U. \quad (13)$$

Here $\alpha > 0$ is an effective Kerr coefficient, and the last term with $M = 2, 3, 4, \dots$ accounts for the M -photon absorption in the optical medium. It is commonly known that, in terms of the polar coordinates (r, θ) , solutions of the linearized equation (13) carrying vorticity S are given by Bessel functions:

$$U = b \exp(ikz + iS\theta) J_S(\sqrt{-kr}), \quad (14)$$

where $k < 0$ is the propagation constant, and b is an arbitrary amplitude. Full equation (13) gives rise to solutions which may be considered as the Bessel modes distorted by the Kerr self-focusing and nonlinear losses. The asymptotic form of the solutions at $r \rightarrow 0$ and $r \rightarrow \infty$ keeps the same form as produced by solution (14) of the linearized equation:

$$U \approx b \exp(ikz + iS\theta) \frac{(\sqrt{-kr})^S}{2^S S!}, \quad ((15a))$$

$$U \approx A \exp(ikz + iS\theta) r^{-1/2} \cos(\sqrt{-kr} + \delta), \quad (15b)$$

where A and δ are amplitude and phase constants.

The weak localization exhibited by Eq. (15b) cannot correspond to a true soliton, because it gives rise to divergence of the respective norm (total-power) integral at $r \rightarrow \infty$:

$$N = 2\pi \int_0^R |U(r)|^2 r dr \simeq \pi A^2 R. \quad (16)$$

On the other hand, the divergence makes it possible to construct stationary solutions to Eq. (13), in spite of the “naive expectation” that the absence of gain terms in the equation does not allow one to compensate the loss. The compensation of the loss in the stationary states generated by Eq. (13) is provided by the influx of power from the infinite reservoir which the Bessel solution keeps at $r \rightarrow \infty$ [56–58]. The local influx rate is determined by the current vector, which is proportional to the squared amplitude and gradient of the local phase:

$$\mathbf{j} = |U|^2 \nabla(\arg(U)). \quad (17)$$

The corresponding compensation condition is tantamount to a local property which all stationary solution share:

$$\nabla \cdot \mathbf{j} + |U|^{2M} = 0. \quad (18)$$

It is relevant to stress the difference of this class of weakly localized solutions and well-localized DSs (such as those displayed, e.g., in Figs. 1-3, 5, 6, and 8). As explained above, DSs exist as isolated states, with uniquely selected values of parameters, including, in particular, the propagation constant. On the contrary to that, the solutions to Eq. (13), specified by b.c. (15a) and (15b), exist for all values of $k < 0$.

These weakly localized solutions with the divergent total power may be stable or unstable, depending on parameters. Examples of stable states with $S = 0$ and 1 are presented in Fig. 9. Stable stationary states with $S = 0$ were observed in an experiment which dealt with light propagation in water [56]. Those weakly localized vortex states which are unstable are split by azimuthal perturbations into steadily rotating fragmented modes (which are similar to *azimuthons*, which were originally introduced in conservative systems [59], and then extended to dissipative ones [60, 61]). An example is presented in Fig. 10.

Numerical solution of Eq. (13) produces stable steadily rotating azimuthons of a different type, which are generated by an input in the form of two slightly mismatched Bessel beams with opposite vorticities, $\pm S$ [62]. In their established form, the azimuthons also represent a species of stable solutions of Eq. (13). An example, fragmented into six segments, is displayed in Fig. 11.

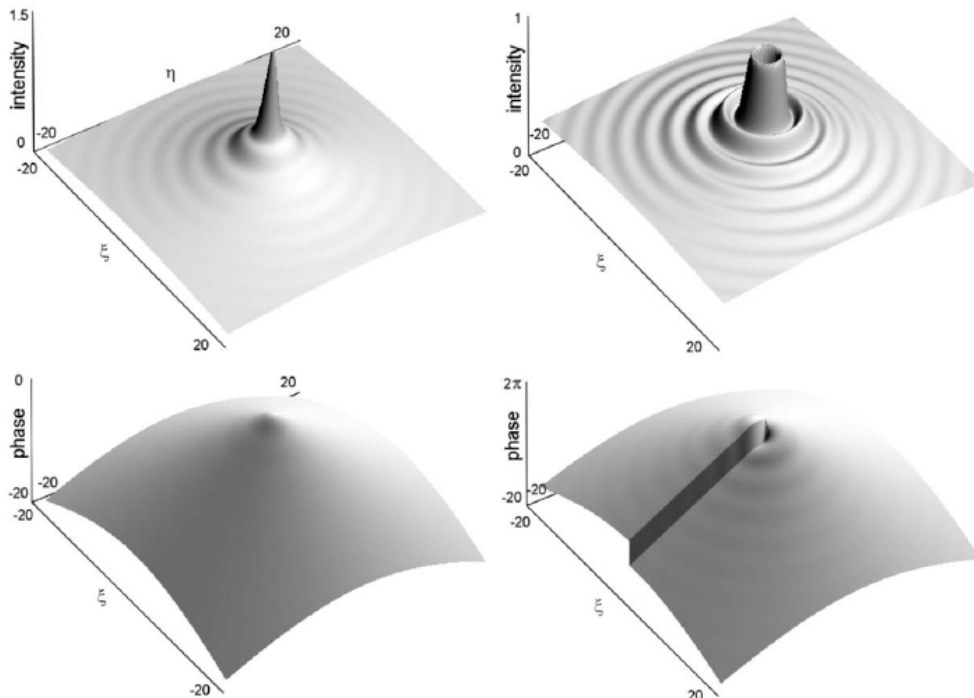


FIG. 9: The left and right columns show the distribution of the local intensity, $|U|^2$ (top panels), and phase, $\arg(U)$ (bottom panels), in stable weakly localized (Bessel-like) modes with $S = 0$ and $S = 1$, respectively. The modes are produced by numerical solution of Eq. (13) with $M = 4$ and $\alpha = 0$ (i.e., the single nonlinear terms represents the higher-order loss). The solutions with $S = 0$ and $S = 1$ correspond, respectively, to $b = 1.174$ and 1.666 in Eq. (15a). The Cartesian coordinates are denoted here as (ξ, η) (source: Ref. [57]).

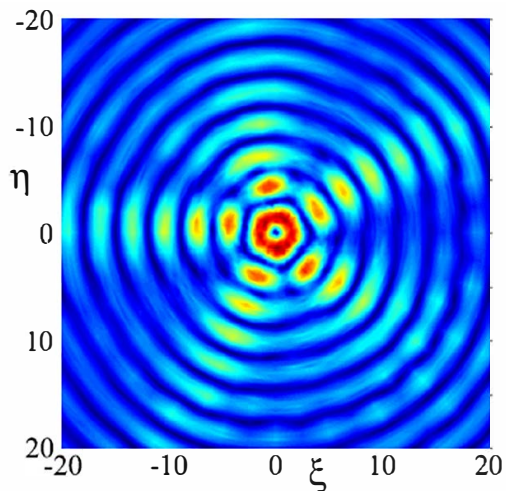


FIG. 10: A rotating fragmented pattern produced by the development of the azimuthal instability of a weakly localized state with vorticity $S = 1$. The result is produced by simulations of Eq. (13) with $M = 4$ and $\alpha = 1.6$. The unstable state is defined by Eq. (15a) with $b = 1.6$ (source: Ref. [58]).

V. LOCALIZED STATES IN 2D NONLINEAR DISSIPATIVE MEDIA WITH SPATIALLY MODULATED GAIN OR LOSS

The use of spatially nonuniform gain or loss offers possibilities for the creation and stabilization of various nonlinear states in the 2D geometry which do not exist or are unstable in uniform dissipative media. This section aims to report

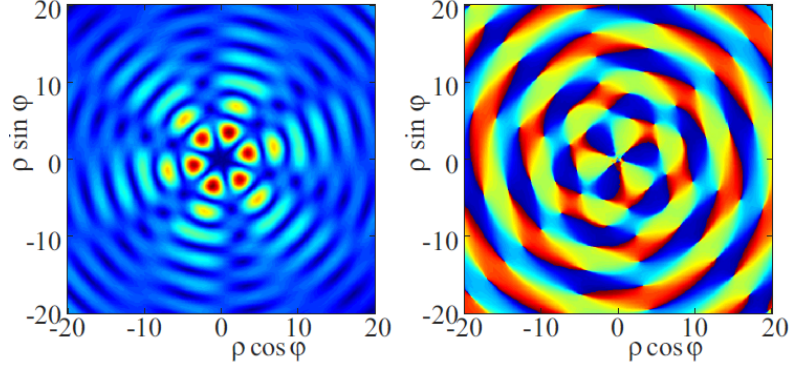


FIG. 11: The intensity and phase distribution in a steadily rotating azimuthon produced by the numerical solution of Eq. (13) with $M = 4$ and $\alpha = 1.6$. The input was taken as a pair of Bessel beams corresponding to $S = \pm 1$, with $b = 1.6$ in Eq. (15a) (source: Ref. [62]).

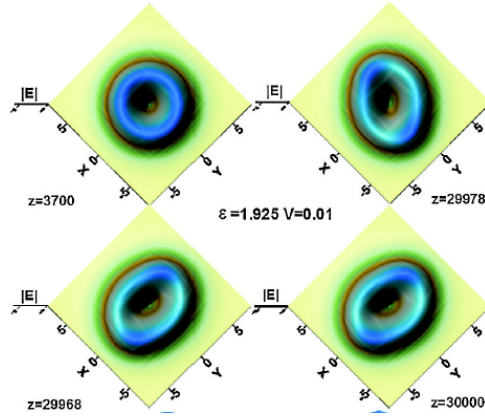


FIG. 12: A stably rotating elliptic vortex, produced by simulations of Eq. (19) with $\gamma = 0.29$, $V = 0.01$, $\varepsilon = 1.925$, $\mu = 1.4$, $\nu = 0.4$. The configurations displayed at $z = 29968$ and $z = 30000$ correspond to the rotation of the ellipse by 180° , hence the rotation period is $\Delta z = 64$ (source: Ref. [43]).

some essential findings produced by analysis of 2D CGL models of this type.

A. Vortex solitons supported by the 2D cubic-quintic CGL equations with spatially modulated linear losses

As mentioned above, the CGL equation (2) with constant coefficients and without the diffusion term ($\beta = 0$) cannot support stable VRs. It was shown [43] that vortex DSs may be stabilized by introducing radial modulation of the linear loss in Eq. (2):

$$\frac{\partial E}{\partial z} = -\delta(r)E + \frac{i}{2} \left(\frac{\partial^2}{\partial x^2} + \frac{\partial^2}{\partial y^2} \right) E + (\varepsilon + i) |E|^2 E - (\mu + i\nu) |E|^4 E, \quad (19)$$

where the modulation format is chosen so as to have the minimum loss at $r = 0$,

$$\delta(r) = \gamma + Vr^2, \quad \text{with } \gamma > 0, V > 0. \quad (20)$$

Systematic numerical analysis of the model based on Eqs. (19) and (20) (which was combined with the variational approximation based on the use of the formal complex Lagrangian of Eq. (19)) gives rise to several species of *stable* localized states with embedded vorticity, depending on values of parameters in Eqs. (19) and (20). First, these may be usual vortex solitons of the crater-shaped-vortex (CSV) type. More interesting are self-trapped vortex modes which spontaneously develop an elliptic shape, that performs rotation at a constant angular velocity around $r = 0$, see an example in Fig. 12.

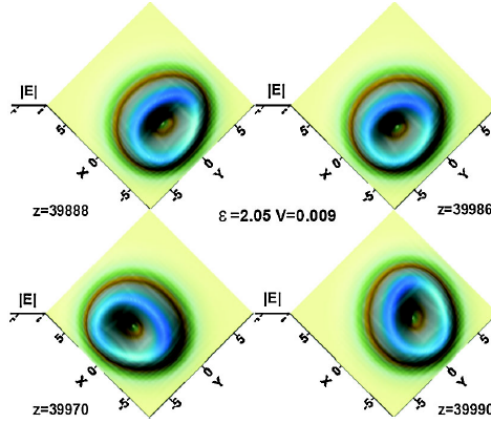


FIG. 13: A stable vortex with the eccentric shape, which combines inner spinning and the orbital motion around the center. The solution is produced by simulations of Eq. (19) with $\gamma = 0.29$, $V = 0.09$, $\varepsilon = 2.05$, $\mu = 1.4$, $\nu = 0.4$. The configurations displayed at $z = 29968$ and $z = 30000$ correspond to the rotation of the ellipse by 180° (source: Ref. [43]).

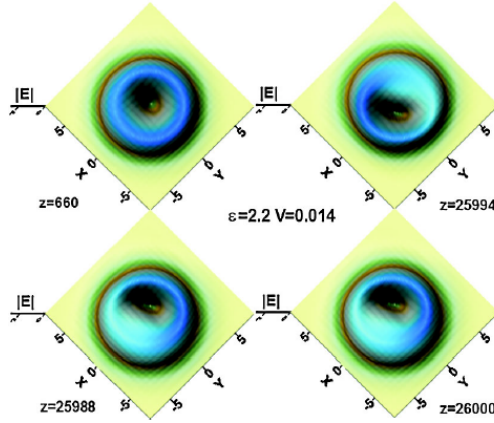


FIG. 14: A stable crescent-shaped spinning vortex, which performs orbital motion around the center. The solution is produced by simulations of Eq. (19) with $\gamma = 0.29$, $V = 0.014$, $\varepsilon = 2.2$, $\mu = 1.4$, $\nu = 0.4$ (source: [43]).

Another stable dynamical mode produced by simulations of Eq. (19) is a still stronger deformed elliptic vortex, which develops an eccentric shape (shifted off the pivot, $r = 0$), as shown in Fig. 13. This vortex features superposition of two modes of rotational motion: spinning around its own center, and precession of the center around the point $r = 0$, with the respective periods locked by ratio 1 : 4.

A still stronger deformation transforms the original isotropic vortex into an internally spinning crescent-shaped one, which also performs precession at a constant angular velocity around the central point. An example of this stable mode is displayed in Fig. 14,

B. Complex modes supported by the 2D cubic-quintic CGL equation with localized linear gain

A natural extension of the above analysis is based on Eq. (19) with modulation format

$$\delta(r) = \gamma - \Gamma r^2. \quad (21)$$

Unlike the format defined above by Eq. (20), expression (21) implies the presence of the linear gain in the circle,

$$r^2 < \gamma/\Gamma. \quad (22)$$

Results of simulations of this model, based on Eqs. (19) and (21), were reported in Ref. [63], fixing, in particular,

$$\gamma = 0.08, \mu = 1.4, \nu = 0.4, \quad (23)$$

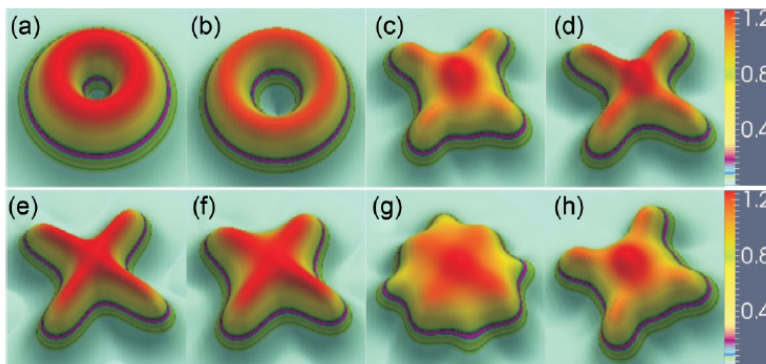


FIG. 15: The evolution of the VR input (panel (a)) governed by Eqs. (19) and (21) with parameters given by Eq. (23) and $\varepsilon = 1.7, \Gamma = 0.018$. First, a vortex soliton is formed, in panel (b). Then, the azimuthal instability breaks the isotropy of the vortex, expels the vorticity, and produces a “Celtic cross” in (c). This is followed by a periodic chain of metamorphoses. Having passed half a period, $\Delta z = 200$, the pattern recovers the Celtic-cross shape (source: [63]).

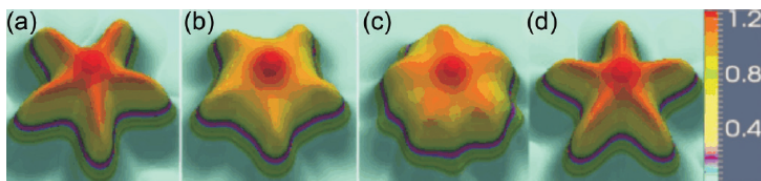


FIG. 16: The periodic chain of metamorphoses of the five-armed star, produced by simulations of Eq. (19) with parameters given by Eqs. (21) and $\varepsilon = 1.7, \Gamma = 0.014$. The period is $\Delta z = 40$. In the course of the evolution the star rotates, so that its angular momentum takes values in interval (24) (source: [63]).

and varying parameters ε (the strength of the cubic gain) and Γ (thus changing the size of the gain area, see Eq. (22)). Actually, ε and Γ are the most essential parameters which determine the selection of various stable states.

The analysis has revealed a great variety of robust localized patterns. First, in a large part of the parameter plane (ε, Γ) , the model produces elliptically deformed rotating vortices similar to those found in the case of the modulation format (20), such as crescent-shaped ones (cf. Fig. 14). More interesting are star-shaped modes into which the vortex input is transformed by the azimuthal modulational instability. In particular, at $\varepsilon = 1.7, \Gamma = 0.018$ the instability development expels the vortex’ pivot (phase singularity), and thus converts the pattern into a cross-shaped one (four-armed star), as shown in Fig. 15. The star performs a cycle of metamorphoses, with half period $\Delta z \approx 200$, as shown in the figure. The computation of the the angular momentum of the pattern, defined by the standard expression, $M = -i \int \int dx dy E^* (x \partial E / \partial y - y \partial E / \partial x)$ (the asterisk stands for the complex conjugate), demonstrates that, in the course of the cyclic evolution, it varies symmetrically between positive and negative values, in an interval of $-0.18 < M < +0.18$ (i.e., the memory of the initial sign of the angular momentum, carried by the VR in Fig. 15(b), is completely lost).

Decreasing Γ to 0.014, the simulations produce a periodically transforming pattern in the form of a five-armed star, which is displayed in Fig. 16. In this case, the periodic metamorphoses occur simultaneously with steady rotation of the star (the cross-shaped pattern observed in Fig. 15 does not rotate). Accordingly, this dynamical state has a definite sign of the angular momentum, which varies in interval

$$-9.7 < M < -8.3. \quad (24)$$

Further decrease of Γ gives rise to star-shaped patterns with the number of arms from six to ten, see an example of the eight-armed star in Fig. 17. All these higher-order modes with the azimuthal structure feature only steady rotation, without a change in their shapes, unlike the metamorphoses exhibited by the four- and five-armed stars.

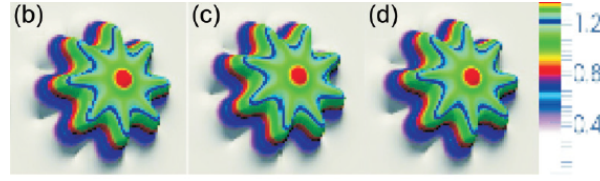


FIG. 17: Steady rotation of the stable pattern shaped as the eight-armed star (without intrinsic metamorphosis, unlike the situations displayed in Figs. 15 and 16), produced by simulations of Eq. (19) with parameters given by Eqs. (21) and $\varepsilon = 1.75, \Gamma = 0.007$. The rotation period is $\Delta z = 192$ (source: [63]).

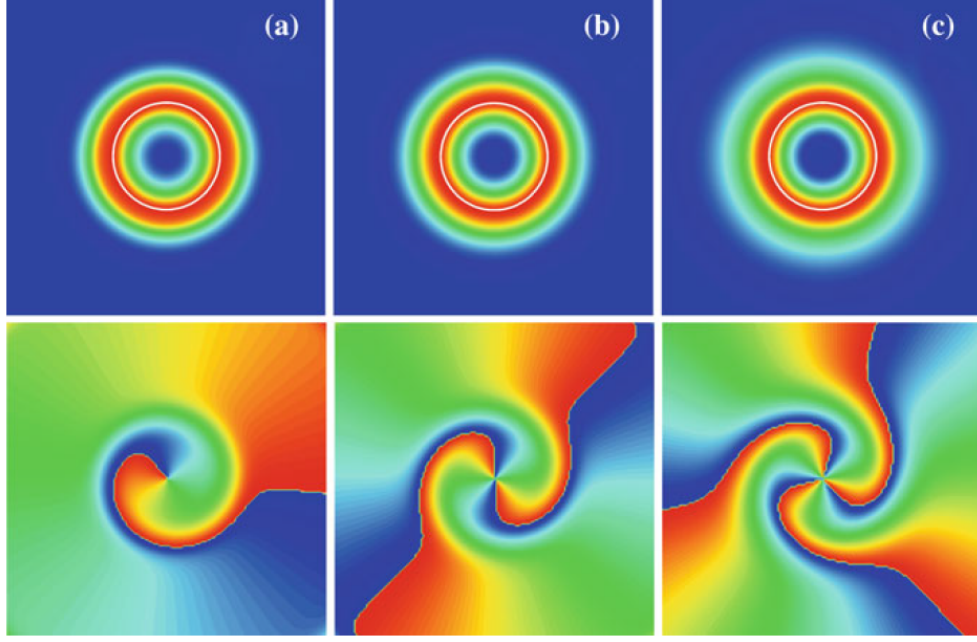


FIG. 18: Distributions of $|U(x, y)|$ and $\arg(U(x, y))$ (the phase of the complex field) in stable vortex solitons with winding numbers $S = 1$ (a), $S = 2$ (b), and $S = 3$ (c), as produced by numerical solution of Eq. (25). White rings designate the location of the local gain maximum, $r = r_0$. The parameters are $\alpha = 2$, $\gamma = 3$, $r_0 = 5.25$, and $d = 1.75$ (source: [44]).

C. Stable vortices supported by the cubic CGL equation with localized gain applied along a ring

It is also natural to consider a possibility to maintain stable localized vortex states by means of localized gain applied along a ring with a finite radius, rather than at the center. This possibility was considered [44] in the framework of the cubic (rather than cubic-quintic, cf. Eq. (19) CGL equation:

$$iU_z + \frac{1}{2}(U_{xx} + U_{yy}) + |U|^2U = i\gamma \exp\left(-\frac{(r-r_0)^2}{d^2}\right)U - i\alpha|U|^2U. \quad (25)$$

The results is that vortices attached to the gain-carrying ring may be stable if γ in Eq. (25) exceeds a certain threshold value, which, in turn, strongly grows with the increase of vorticity S . Examples of stable vortical modes with winding numbers $S = 1, 2$, and 3 are displayed in Fig. 18.

Stable VRs supported by a similar ring-shaped local gain configuration, but in the system of two dissipative equations for the fundamental-frequency and second-harmonic waves coupled by the $\chi^{(2)}$ (quadratic) nonlinearity were recently reported too [64].

VI. TWO-DIMENSIONAL DSS (DISSIPATIVE SOLITONS) IN THE HO (HARMONIC-OSCILLATOR) TRAPPING POTENTIAL

A. The CGL equation with the CQ nonlinearity and linear loss

As mentioned above, the CGL equation (2), which is relevant as a model in optics, does not include the diffusion term, i.e., it has $\beta = 0$. Then, the problem is that vortex-soliton solutions of such an equation with constant coefficients are completely unstable. In addition to what is considered above (spatial modulation of the linear loss/gain), dissipative-VR solutions can be stabilized by means of a trapping potential [41, 65], the most natural form of which is the HO potential,

$$U(r) = (\Omega^2/2) r^2. \quad (26)$$

Thus, the corresponding form of Eq. (19), which includes potential (26), is

$$\frac{\partial E}{\partial z} = -\delta \cdot E + \frac{i}{2} \left(\frac{\partial^2}{\partial x^2} + \frac{\partial^2}{\partial y^2} \right) E + (\varepsilon + i) |E|^2 E - (\mu + i\nu) |E|^4 E - \frac{i}{2} \Omega^2 r^2 E. \quad (27)$$

As shown in Ref. [41], adequate results can be obtained, in particular, by fixing

$$\delta = 0.5, \mu = 1, \nu = 0.1, \quad (28)$$

while the most important parameters, *viz.*, the cubic gain ε and HO-trap strength Ω^2 , are subject to variation.

Stationary axisymmetric solutions of Eq. (27) with a real propagation constant k and integer vorticity S can be looked for in the usual form, using the polar coordinates (r, θ) :

$$E(x, y, z) = \exp(ikz + iS\theta) U(r), \quad (29)$$

where complex function $U(r)$ satisfies the radial equation,

$$\left(\delta + ik + \frac{i}{2} \Omega^2 r^2 \right) U = \frac{i}{2} \left(\frac{d^2}{dr^2} + \frac{1}{r} \frac{d}{dr} - \frac{S^2}{r^2} \right) U + (\varepsilon + i) |U|^2 U - (\mu + i\nu) |U|^4 U. \quad (30)$$

Appropriate numerical solutions of both equations (27) and (30) could be found starting with a straightforward form of the input,

$$U_0(r) = A_0 r^{|S|} \exp(-r^2/w_0^2), \quad (31)$$

with amplitude A_0 and w_0 . The stationary solutions are characterized, as usual, by values of the integral power (norm),

$$P = 2\pi \int_0^\infty |U(r)|^2 r dr. \quad (32)$$

Values of k were found as eigenvalues at which Eq. (30) produces appropriate solutions for $U(r)$.

Numerical solutions with $S = 1$ readily produce stable solutions in the form of CSVs, see a typical example in Fig. 19. The amplitude and phase structures of the stable CSV with $S = 1$ are displayed, at slightly different values of parameters, in Fig. 20. As expected, its shape shows a spiral structure.

The results are summarized in Fig. 21(b) by means of plots which show curves $P(\varepsilon)$ for power (32) vs. the cubic gain, at different fixed values of the trapping strength, Ω , for families of the CSV solutions, distinguishing stable and unstable solutions. In accordance with what is stated above, the vortices are completely unstable if the trapping potential is absent or too weak, $\Omega \leq 1$. The stability region attains its maximum close to $\Omega = 1.6$. This is a value at which the characteristic radial size, determined by the HO potential,

$$r_{\text{HO}} = \Omega^{-1/2}, \quad (33)$$

is roughly equal to the natural width of the 2D solitons created by the CQ-CGL equation. When the further increase of Ω makes the trapping potential too tight, the stability region gradually shrinks. For the sake of comparison, similar curves $P(\varepsilon)$ for fundamental DSS, with $S = 0$, are presented in Fig. 21(a). It is seen that the stability region of the fundamental DSS monotonously shrink with the increase of Ω .

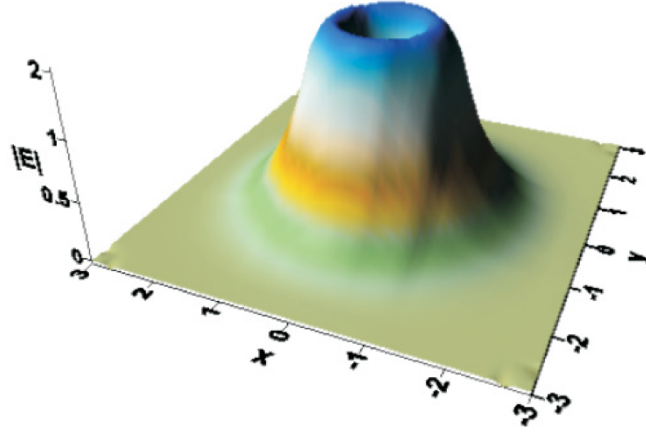


FIG. 19: The profile of $|E(x, y)|$ for the stable stationary solution of Eq. (27) in the form of the CSV (crater-shaped vortex), with winding number $S = 1$, see Eq. (29)). The parameters are taken as per Eq. (28), along with $\varepsilon = 2.22$ and $\Omega = 1.7$ (source: [41]).

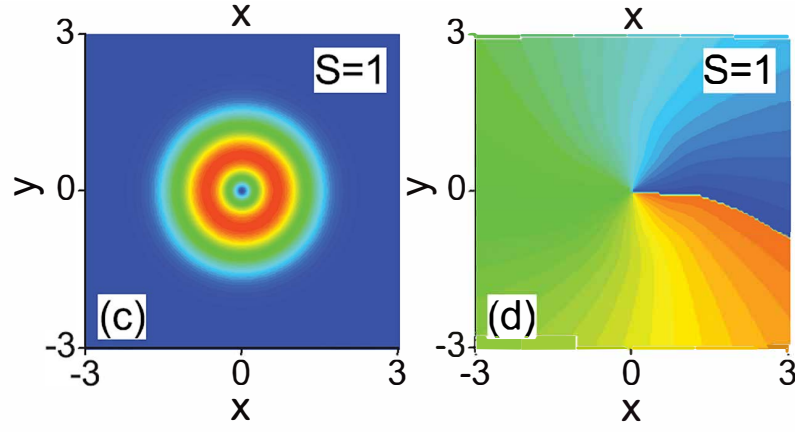


FIG. 20: The left and right panels display, respectively, the top view of amplitude $|E(x, y)|$ and a snapshot of the phase, $\arg(E(x, y))$, of the stable stationary solution of Eq. (27) in the form of the CSV with $S = 1$. The parameters are taken as per Eq. (28), along with $\varepsilon = 1.8$ and $\Omega = 2$ (source: [41]).

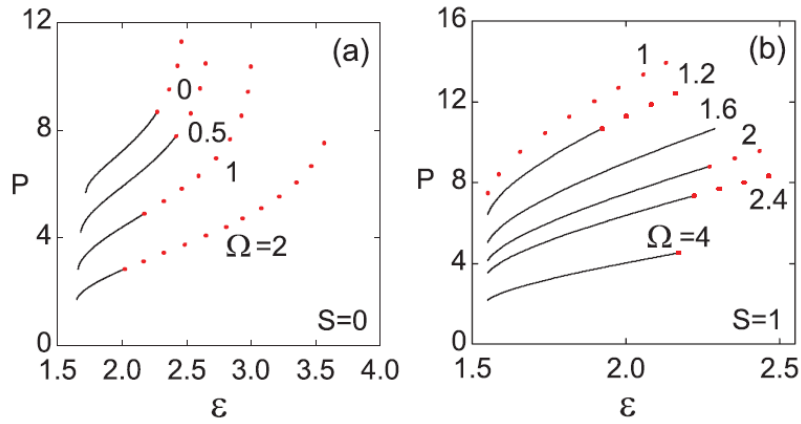


FIG. 21: Panels (a) and (b) show dependences of the integral power (32) on the cubic gain, ε , in Eq. (27), at different fixed values of strength Ω of the HO trap, for families of fundamental ($S = 0$) and VR ($S = 1$) states, respectively. Other parameters are fixed as in Eq. (28) (source: [41]).

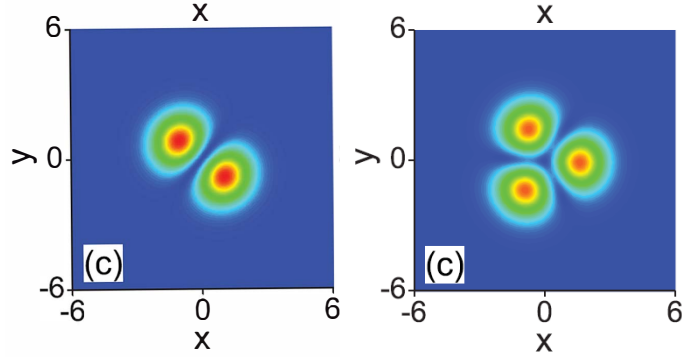


FIG. 22: The left and right panels show examples of dipoles and tripoles, produced by the spitting instability of the CSV states with $S = 1$ and 2 , respectively. The parameters are $\varepsilon = 1.8$, $\Omega = 0.5$ in (a), and $\varepsilon = 1.7$, $\Omega = 0.5$ in (b). Other parameters are fixed as in Eq. (28) (source: [41]).

Those CSV states with $S = 1$ which are unstable spontaneously split into stable dipole modes, as shown in the left panel of Fig. 22. As concerns the CSVs with $S = 2$, they can be easily obtained as stationary solutions (using Eq. (30)), but simulations of Eq. demonstrate that they all are unstable, spontaneously splitting into *tripoles* which, by themselves, are stable states, see an example in the right panel Fig. 22. Further simulations demonstrate that the emerging dipoles are static modes, while the tripoles feature rotation at a constant angular speed. In fact, both dipoles and tripoles can be directly constructed as solutions of Eq. (30) (for the tripoles, it should be rewritten as the stationary equation in the rotating reference frame).

B. The cubic CGL equation with linear gain

As mentioned above, the CGL equation normally generates stable localized solutions if it includes the linear loss, which secures the stability of the zero background around the localized state. Nevertheless, the equation which combines the *linear gain*, diffusion term, and the HO trapping potential also admits stable solutions, because small perturbations fueled by the linear gain far from the soliton roll down the HO potential profile towards the location of the soliton, where the cubic loss helps to suppress them. In this case, the presence of the linear gain requires the inclusion of the cubic loss, while quintic terms are not necessary, which makes the CGL equation essentially simpler [66]:

$$i \frac{\partial \psi}{\partial t} = -\frac{1}{2}(1 - i\eta) \left(\frac{\partial^2}{\partial x^2} + \frac{\partial^2}{\partial y^2} \right) \psi - \sigma |\psi|^2 \psi + i\gamma(1 - |\psi|^2)\psi + \frac{1}{2}\Omega^2 r^2 \psi, \quad (34)$$

cf. Eq. (27). Equation (34) is written as the dissipative Gross-Pitaevskii equation for the exciton field in a 2D semiconductor microcavity. Here γ is the linear gain (the coefficient of the cubic loss is made equal to γ by means of scaling), η is the diffusion coefficient (the same as β in Eq. (2)), and $\sigma = +1$ or $= -1$ for the self-focusing or defocusing cubic term, respectively.

At the threshold of emergence of nontrivial solutions with an infinitesimal amplitude ε , real chemical potential μ and integer vorticity $S \geq 0$, in the form of

$$\psi(x, y, t) = \varepsilon u_{\text{thr}}(r) \exp(-i\mu t + iS\theta), \quad (35)$$

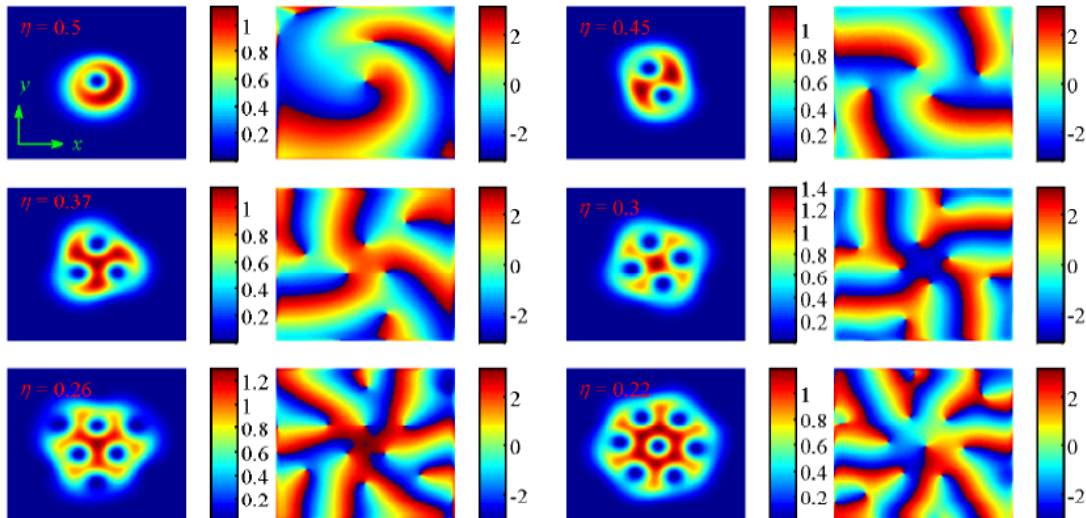
complex function $u(r)$ satisfies the linearized equation which follows from the substitution of ansatz (35) in Eq. (34):

$$\mu u_{\text{thr}} = -\frac{1}{2}(1 - i\eta) \left(\frac{d^2}{dr^2} + \frac{1}{r} \frac{d}{dr} - \frac{S^2}{r^2} \right) u_{\text{thr}}(r) + i\gamma u_{\text{thr}}(r) + \frac{1}{2}\Omega^2 r^2 u_{\text{thr}}(r). \quad (36)$$

This equation admits the *exact solution*,

$$u_{\text{thr}}(r) = r^S \exp\left(-\frac{\Omega}{2\sqrt{1 - i\eta}} r^2\right), \quad (37)$$

FIG. 23: A sequence of stably rotating states (patterns of the local intensity, $|u(x, y, t)|^2$, and local phase, $\arg(u(x, y, t))$, are shown), which were produced by simulations of Eq. (34) with $\sigma = +1$, $\gamma = 2.5$, and $\Omega^2 = 2$, at decreasing values of diffusivity η , which are indicated in the panels. The sequence includes a crescent vortex ($S = 1$), and multi-vortex complexes with $S = 2, 3, 4, 6$, and 7. The rotation angular velocities are $\omega(S = 1) \approx 3.9$, $\omega(S = 2) \approx 1.7$, $\omega(S = 3) \approx 1.6$, and $\omega(S = 4, 6, 7) \approx 1.5$. At $\eta > 0.5$, the model supports a stable axisymmetric vortex with $S = 1$, while at $\eta < 0.22$ a transition to vortex turbulence occurs. (source: Ref. [66]).



with chemical potential

$$\mu_{\text{thr}} = \frac{(1+S)\Omega\eta}{\sqrt{2(\sqrt{1+\eta^2}-1)}}, \quad (38)$$

at the threshold value of the linear gain:

$$\gamma_{\text{thr}} = (1+S)\Omega\sqrt{\frac{1}{2}(\sqrt{1+\eta^2}-1)}. \quad (39)$$

This result means that, for given η , nontrivial states with vorticity S exist at $\gamma > \gamma_{\text{thr}}$.

Fixing the value of the linear gain, e.g., $\gamma = 2.5$, numerical solution of Eq. (34) with $\Omega^2 = 2$ and $\sigma = +1$ gives rise to a stable solution in the form of an axisymmetric vortex with $S = 1$ at $\eta > 0.5$. Making the system “more agile” by decreasing η , it was observed that, as shown in Fig. 23, at $\eta = 0.5$, the axisymmetric vortex is replaced by a rotating deformed one, with a crescent-like shape of the intensity pattern. At still smaller values of η , the single vortex passes a cascade of splittings. As a result, the role of the stable state is played, consecutively, by rotating clusters of 2, 3, 4, 6, and 7 vortices. Finally, the system falls into a state of vortex chaos (“turbulence”) at $\eta < 0.22$.

Note that the sequence of the rotating patterns displayed in Fig. 23 does not include a cluster of five vortices. Such a stable state is produced too by the simulations of Eq. (34) with $\sigma = -1$ (the self-defocusing cubic term).

For the case of $\sigma = 0$, when the nonlinearity is represented, in Eq. (34), solely by the cubic loss, the results are summarized in the stability chart plotted in Fig. 24 in the plane of parameters (γ, η) . Note, in particular, that the exact analytical result (39) correctly predicts the boundary of the existence of nontrivial states.

VII. DISSIPATIVE VORTEX SOLITONS STABILIZED BY SPATIALLY PERIODIC (LATTICE) POTENTIALS

A. Crater-shaped (tightly confined) vortex solitons

It is known that the conservative 2D NLS equation with the CQ nonlinearity and a spatially periodic (lattice) potential cannot produce stable vortical modes (“eddies”) of the CSV type, that would be essentially “squeezed” in

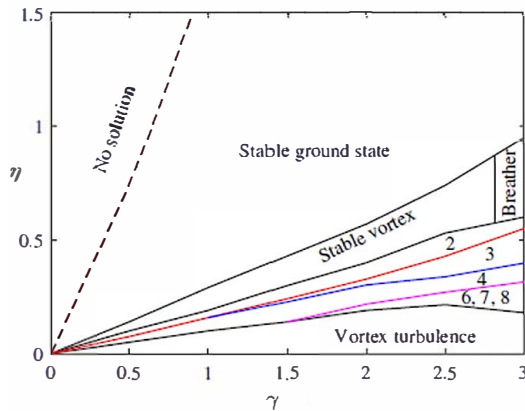


FIG. 24: Stability borders of different patterns in the plane of (γ, η) for $\sigma = 0$ and $\Omega^2 = 1$, produced by the numerical solution of Eq. (34). The analytical existence boundary, predicted by Eq. (39), and its numerically identified counterpart completely overlap, in the form of the dashed line. Digits in subregions represent the number of vortices in rotating clusters populating these subregions. In particular, 1 implies the presence of the single ($S = 1$) rotating crescent-shaped vortex, different from the axisymmetric one in the area of “Stable vortex”. Label “Breather” identifies a small region in which the dominant state is one with $S = 0$ which performs regular internal oscillations (source: [66]).

a single cell of the lattice [67]. Nevertheless, the CQ-CGL equation with the same spatially-periodic potential, which does not include the diffusion term ($\beta = 0$ in the corresponding equation (2)), can produce stable eddies of the CSV type [41]. The respectively modified equation (27) is

$$\frac{\partial E}{\partial z} = -\delta \cdot E + \frac{i}{2} \left(\frac{\partial^2}{\partial x^2} + \frac{\partial^2}{\partial y^2} \right) E + (\varepsilon + i) |E|^2 E - (\mu + i\nu) |E|^4 E - ip [\cos(2x) + \cos(2y)] E. \quad (40)$$

Here coordinates (x, y) are scaled so that the period of the lattice potential with amplitude $p > 0$ is π . The form of the potential adopted in Eq. (40) implies that point $x = y = 0$ corresponds to a local maximum of the potential, rather than a minimum. This definition is natural if the intention is to produce CSV solutions, with the zero amplitude (vortex’ pivot) which should be placed at a local potential maximum.

The numerical solution of Eq. (40) readily produces stationary states of the CSV type, a part of which are stable. A typical example of a stable CSV solution is displayed in Fig. 25. The results are summarized in Fig. 26 which presents families of stable CSV solutions by dint of the dependence of its integral power,

$$P = \int \int |E(x, y)|^2 dx dy \quad (41)$$

(cf. Eq. (32)), on the cubic-drive’s strength, ε .

CSV modes with winding number $S = 2$ can be found too, as stationary solutions of Eq. (40), but they all are unstable. Spontaneous development of the instability transforms them into stable quadrupoles, as shown in Fig. 27. Such localized quadrupoles also constitute families of stable solutions.

A relevant extension of the analysis of the model based on Eq. (40) is to study a possibility of setting DSs in motion by kicking them. A critical strength of the kick leading to depinning of a soliton originally pinned to the underlying potential lattice, and various scenarios of complex pattern formation, following the depinning and also collisions between traveling DSs, were studied by means of systematic simulations by in Ref. [69].

B. Multi-peak vortex solitons

When the CSV solutions of the conservative NLS equation with the 2D lattice potential are unstable, the same equation can easily give rise to stable rhombus- and square-shaped solutions, built of four local peaks, which carry the phase pattern corresponding to vorticity $S = \pm 1$. Such onsite (OS)-centered [70] and intersite (IS)-centered [71] multi-peak vortex complexes are well known as stable solutions of the 2D conservative NLS equation with the lattice potential, see also the review . The CGL equation (40) produces similar multi-peak vortex states, as shown by Leblond, Malomed, and Mihalache (2009). As a typical set of parameter values which makes it possible to find stable

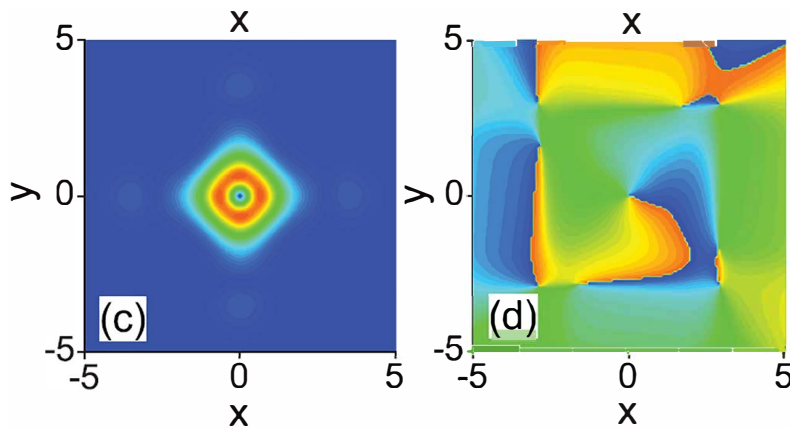


FIG. 25: The left and right panels display the amplitude and phase distribution of a stable “crater-shaped” vortex (CSV) with winding number $S = 1$, as produced by the numerical solution of Eq. (40). The CSV is essentially squeezed in a single cell of the potential lattice with strength $p = 2$ and cubic-gain coefficient $\varepsilon = 2$. Other parameters of Eq. (40) are fixed as in Eq. (28) (source: Ref. [41]).

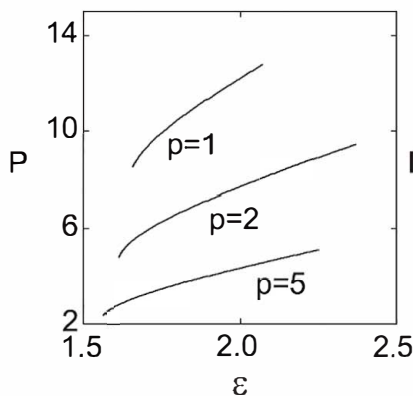


FIG. 26: Dependence of the integral power (41) of the CSVs (crater-shaped vortices) with $S = 1$ on the cubic-gain coefficient, ε , produced by the numerical solution of Eq. (40) at indicated fixed values of strength p of the lattice potential. Other parameters are fixed as in Eq. (28) (source: Ref. [41]).

compound-vortex modes, one can take

$$\delta = 0.4, \varepsilon = 1.85, \mu = 1, \nu = 0.1, V_0 \equiv -p = 1. \quad (42)$$

Note that the negative sign of $p \equiv -V_0$ in Eq. (42) implies that, unlike the situation illustrated above by Figs. 25-27, the central point, $x = y = 0$, is a local minimum of the cellular potential (rather than a maximum).

A set of top-view plots of $|E(x,y)|$ for the stable OS-centered vortex rhombuses are displayed in Fig. 28. In particular, the difference between the left and central panels is that the quintic self-interaction, represented by coefficient ν , is, respectively, focusing ($\nu < 0$) and defocusing ($\nu > 0$) in them. Accordingly, the pattern in the left panel is essentially more self-compressed than in the central one.

Families of the OS-centered vortex complexes are characterized in Fig. 29 by dependences of their integral power, calculated according to Eq. (41), and propagation constant (found as the eigenvalue of Eq. (40)) on the cubic-gain coefficient ε . It is seen that the rhombic vortices are unstable if ε is too small or too large, being stable in the broad intermediate region.

An example of the amplitude and phase structure in a stable IS-centered (square-shaped) vortex complex is displayed in Fig. 30. In particular, the phase pattern clearly corroborates the presence of vorticity $S = 1$ in this complex.

In addition to the OS- and IS-centered vortex complexes, Eq. (40) generates stable compound states in the form of *quadrupoles*, which do not carry vorticity. An example of an OS-centered one (a rhombic quadrupole) is displayed in Fig. 31. These solutions also form families parameterized by values of the cubic gain ε , cf. Fig. 29.

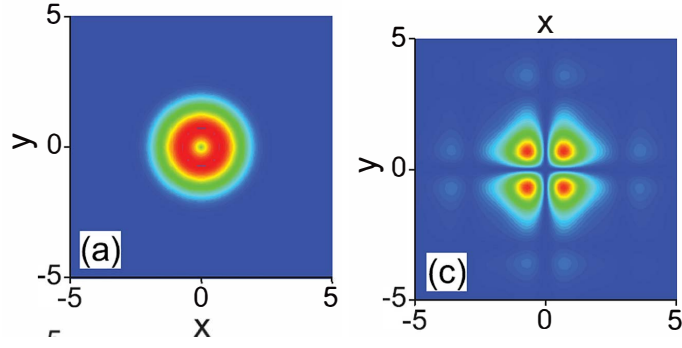


FIG. 27: (a) The amplitude profile of an unstable CVS model with winding number $S = 2$, obtained as a numerical solution of Eq. (40) with $\varepsilon = 1.8$ and $p = 2$. Other parameters are fixed as in Eq. (28). (c) The amplitude profile of a stable quadrupole into which the unstable vortex from (a) is transformed by the development of the instability (source: Ref. [41]).

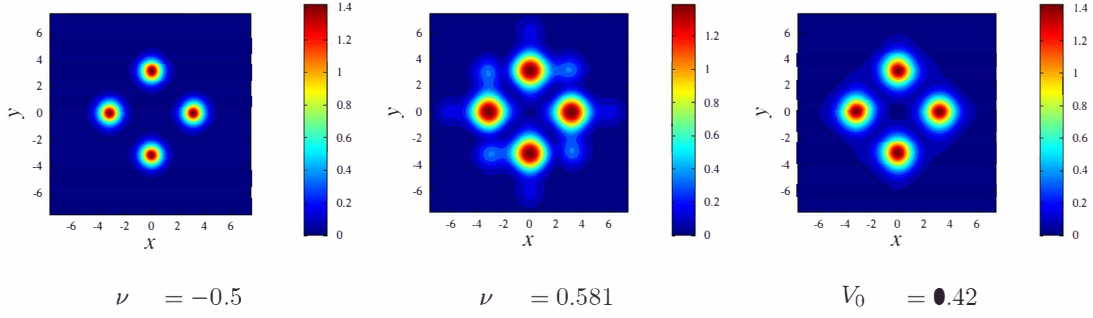


FIG. 28: Patterns of $|E(x, y)|$ in stable OS-centered (rhombus-shaped) four-peak vortex complexes with winding number $S = 1$, obtained as numerical solutions of Eq. (40) with parameters taken as per Eq. (42), except for ν (in the left and central panels) or V_0 (in the right one), whose values are indicated in the figure (source: Ref. [42]).

C. Dissipative gap solitons (GSs) generated by the CGL equation with the 2D lattice potential

The results presented above are based on the CGL equation (40) with the self-focusing cubic nonlinearity. It is also interesting to consider the model with the self-defocusing cubic term. It is well known that the respective 2D conservative NLS equation with the lattice potential gives rise to families of gap solitons (GSs) [72, 73].

GSs as solutions of the 1D CGL equation with the lattice potential were introduced in Ref. [74]. The 2D setting was then developed in Ref. [75], where the CGL equation with the 2D lattice potential was adopted in the following

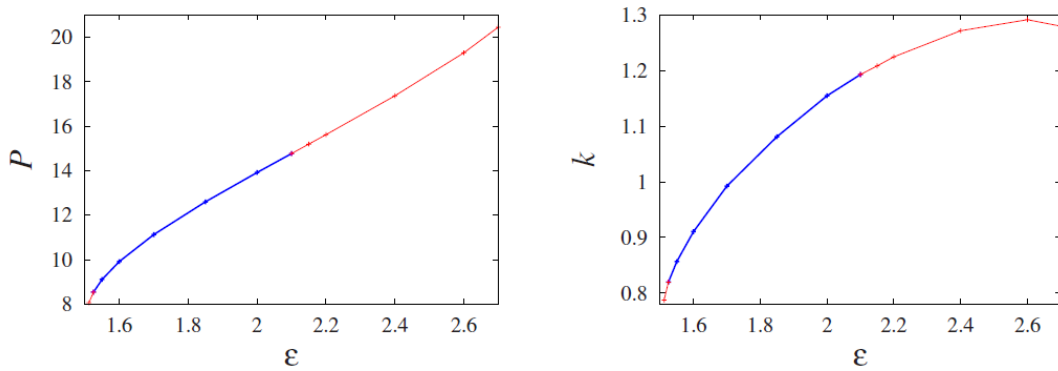


FIG. 29: Dependence of the integral power (41) and propagation constant k (the eigenvalue of Eq. (40)) for the family of OS-centered vortex complexes, built of four peaks (see Fig. 28), on strength ε of the cubic gain. Blue (lower) and red (upper) segments denote, respectively, stable and unstable subfamilies (source: Ref. [42]).

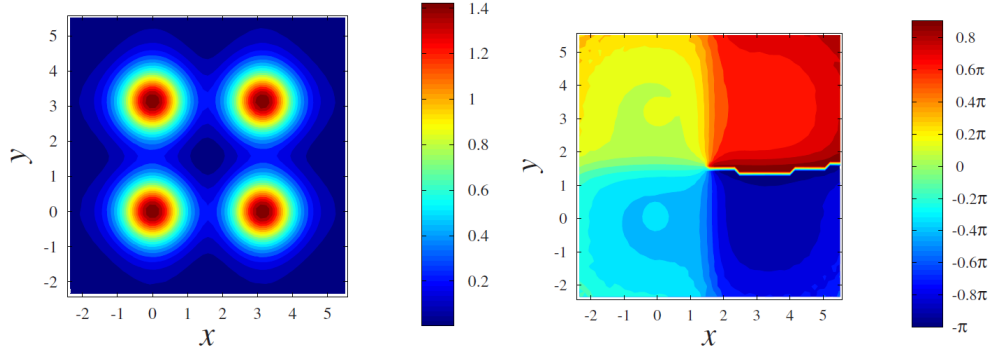


FIG. 30: Amplitude and phase patterns of a stable IS-centered (square-shaped) vortex complex with winding number $S = 1$, obtained as a numerical solution of Eq. (40) with parameters taken as per Eq. (42) (source: Ref. [42]).

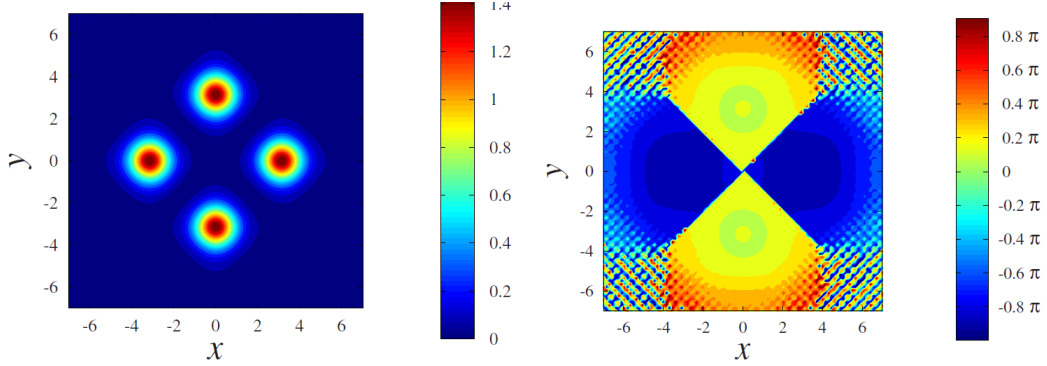


FIG. 31: Amplitude and phase patterns of a stable OS-centered (square-shaped) quadrupole, produced by the numerical solution of Eq. (40) with parameters taken as per Eq. (42) (source: Ref. [42]).

form, which does not include the diffusion term (recall that term is irrelevant for realizations in optics):

$$\left(\frac{\partial}{\partial z} + \Gamma_1\right)\psi = \frac{i}{2}\left(\frac{\partial^2}{\partial x^2} + \frac{\partial^2}{\partial y^2}\right)\psi - i|\psi|^2\psi + iA\{\cos(2q_0x) + \cos(2q_0y)\}\psi + (\Gamma_2|\psi|^2 - \Gamma_3|\psi|^4)\psi. \quad (43)$$

In comparison to Eq. (40), this CGL equation does not include the quintic conservative term, which is not essential in the present context, and, with $A > 0$, the point $x = y = 0$ is a minimum of the potential.

Assuming that the loss and gain coefficients $\gamma_{1,2,3}$ in Eq. (43) are small parameters, an analytical approximation for constructing DS solutions was developed in Ref. [75]. To this end, Eq. (43) was, at first, considered in the conservative limit, with $\gamma_{1,2,3} = 0$, in which case Eq. (43) has the usual Lagrangian. Using this fact, the variational approximation was elaborated for the fundamental solitons, adopting the following ansatz:

$$\psi_{\text{fund}} = B \exp\left(ikz - \frac{x^2 + y^2}{2W^2}\right) \cos(qx) \cos(qy), \quad (44)$$

where amplitude A and width W are variational parameters, q being an adjustment constant. In the zero-order approximation with respect to the loss and gain terms, $\gamma_{1,2,3} = 0$, the integral power (norm) of ansatz (44),

$$P = \iint |\psi(x, y)|^2 dx dy = (\pi/4)B^2W^2 [1 + \exp(-q^2W^2)]^2, \quad (45)$$

is an arbitrary parameter of the soliton family. Then, the loss and gain are taken into regard by means of the balance equation for the power, which, by itself, is an exact corollary of Eq. (43):

$$\frac{dP}{dz} = 2\left(-\Gamma_1P + \Gamma_2 \iint |\psi|^4 dx dy - \Gamma_3 \iint |\psi|^6 dx dy\right). \quad (46)$$

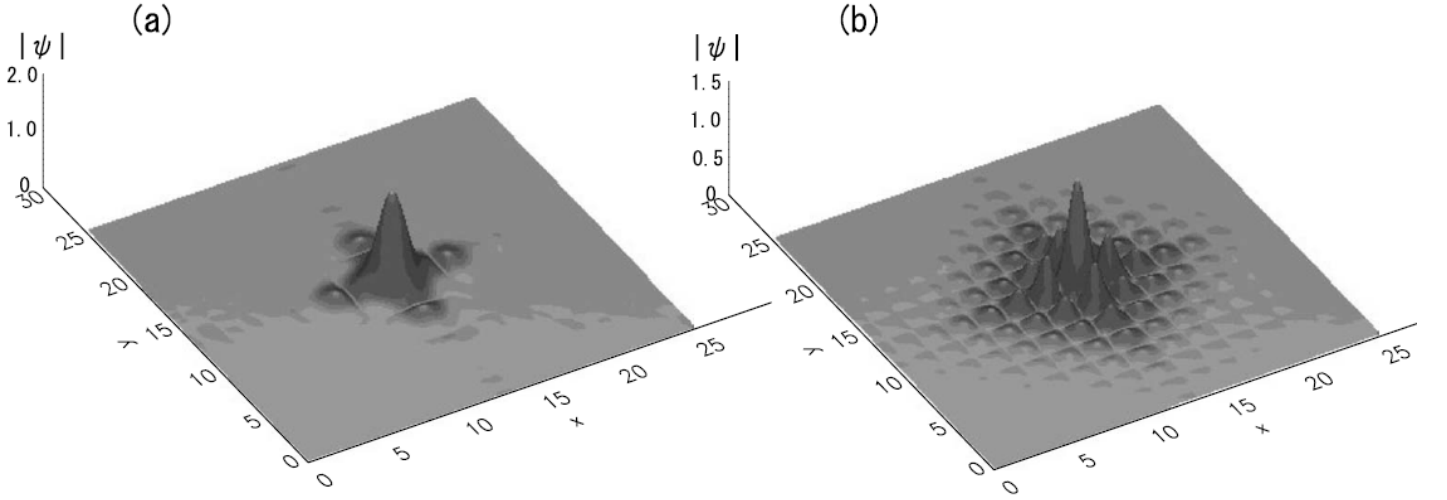


FIG. 32: Shapes of $|\psi(x, y)|$ in stable fundamental solitons, produced as numerical solutions of Eq. (43) with parameters $A = 2$, $\Gamma_1 = 0.025$, $\Gamma_2 = 0.1$, $\Gamma_3 = 0.05$ and $q_0 = 1$ in (a) (a tightly bound soliton), and $q_0 = 1.75$ in (b) (a loosely bound soliton). Source: Ref. [75].

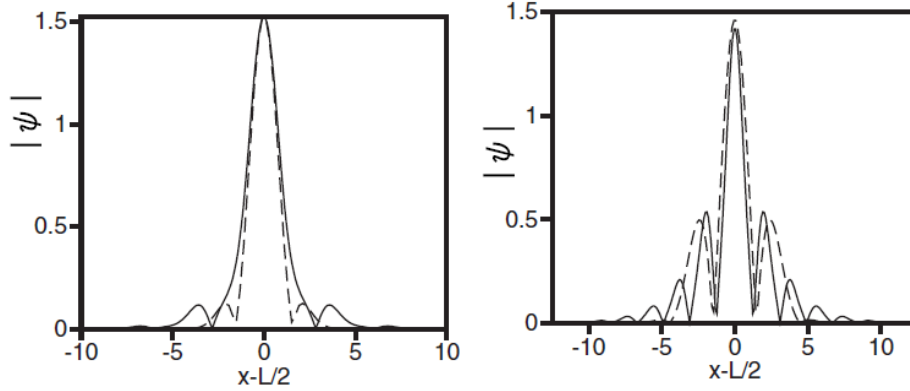


FIG. 33: Solid lines in the left and right panels show cross sections of the 2D profiles of the same fundamental dissipative GSs (tightly and loosely bound ones, respectively) which are displayed in Figs. 32(a) and (b). Dashed lines depict the analytical prediction of the VA based on ansatz (44), with $q = 1$ and 1.05 , in the left and right panels, respectively, and the balance condition $dP/dz = 0$, as it follows from Eq. (46) (source: Sakaguchi and Malomed (2009)).

Finally, the stationary solution of the CGL equation is analytically predicted as one corresponding to $dP/dz = 0$ in Eq. (45).

Similar to their counterparts produced by the conservative NLS equation [73], GS solutions of the CGL equation (43) also feature loosely and tightly bound shapes. Examples of stable GSs of these types are shown in Fig. 32. Their shapes are additionally illustrated, and compared to the analytical approximation outlined above, in Fig. 33.

Numerical results for the fundamental dissipative GSs are summarized in the stability chart in the parameter plane of $\gamma_1 \equiv 20\Gamma_1$ (the linear-loss coefficient and A (it determines depth $4A$ of the lattice potential in Eq. (43)), which is presented in Fig. 34. Naturally, stable GSs exist if the underlying potential is strong enough.

Vortex-soliton solutions with winding number $S = 1$ were produced by the numerical solution of Eq. (43) with input

$$(\psi_{\text{vort}})_0 = B(x + iy) \exp\left(-\frac{x^2 + y^2}{2W^2}\right) \cos(qx) \cos(qy), \quad (47)$$

varying parameters B , W , and q . The results are stable vortex solitons of the same two types as identified in the case of the fundamental solitons, i.e., loosely and tightly bound ones. Examples are presented in Fig. 35.

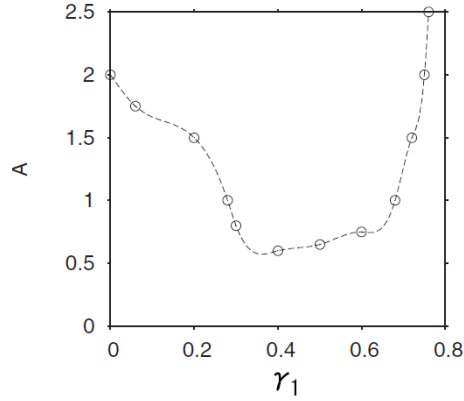


FIG. 34: Stable fundamental dissipative GSs exist, as solutions to Eq. (43), above the plotted boundary in the parameter plane ($20\Gamma_1, A$). Other parameters are $\Gamma_2 = 0.1$, $\Gamma_3 = 0.05$, and $q_0 = 1$ (source: Sakaguchi and Malomed (2009)).

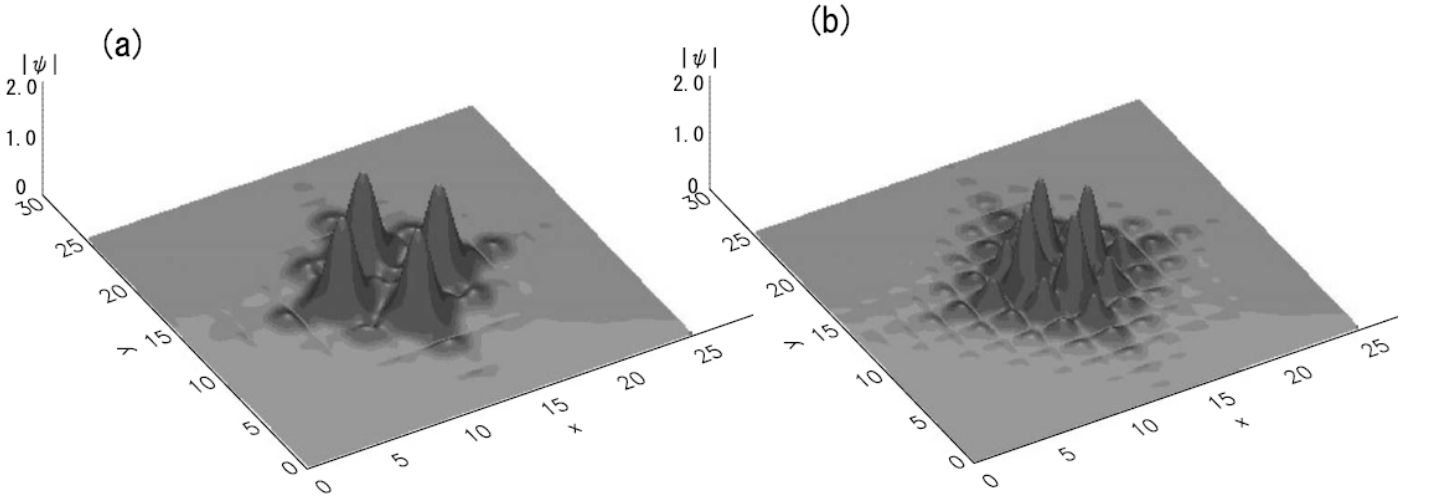


FIG. 35: Shapes of $|\psi(x, y)|$ in stable vortex solitons with $S = 1$, produced as numerical solutions of Eq. (43) with parameters $A = 2$, $\Gamma_1 = 0.025$, $\Gamma_2 = 0.1$, $\Gamma_3 = 0.05$ and $q_0 = 1$ in (a) (a tightly bound vortex soliton), and $q_0 = 1.6$ in (b) (a loosely bound one). Source: Ref. [75].

VIII. TWO-COMPONENT DISSIPATIVE SOLITONS OF THE VORTEX-ANTIVORTEX (VAV) TYPE STABILIZED BY SOC (SPIN-ORBIT COUPLING)

A. The model

Parallel to the well-known work aimed at the emulation of SOC in binary BEC mixtures [76], SOC effects were realized in exciton-polariton fields populating semiconductor microcavities [77–81]. Actually, SOC in polaritonic microcavities may have two different physical origins, *viz.*, the direct SOC acting on excitons, or SOC mixing two photonic modes. The latter option makes it possible to realize SOC in microcavities operating in the regime of weak coupling between light and matter, when polaritons are not formed, while SOC originates from the splitting of cavity modes, ψ_{\pm} , whose electric-field components are perpendicular (TE) and parallel (TM) to the in-plane component of the carrier wave vector.

Here, this option is addressed, following Ref. [82]. To this end, a planar waveguide is considered with saturable gain and saturable absorption, which are provided by laser setups [2, 34, 83–86]. The corresponding system of coupled CGL equations, including scaled time t and in-cavity coordinates x and y , is

$$i\partial_t\psi_+ = -(\partial_x^2 + \partial_y^2)\psi_+ + if\psi_+ + \beta(\partial_x - i\partial_y)^2\psi_-, \quad (48)$$

$$i\partial_t\psi_- = -(\partial_x^2 + \partial_y^2)\psi_- + if\psi_- + \beta(\partial_x + i\partial_y)^2\psi_+, \quad (49)$$

$$f = -1 + \frac{g}{1 + \varepsilon(|\psi_+|^2 + |\psi_-|^2)} - \frac{a}{1 + (|\psi_+|^2 + |\psi_-|^2)}. \quad (50)$$

Here the coefficient of the linear loss is scaled to be 1, the saturable gain and absorption are represented, respectively, by coefficients $g > 0$ and $a > 0$, and SOC is represented by terms with coefficient β , which perform linear mixing between the modes via the second spatial derivatives [87], unlike the first derivatives which represent SOC in the BEC models [76]. Further, positive $\varepsilon < 1$ defines relative saturation strength of the gain and absorption in Eq. (50). The generic situation may be adequately represented by parameters

$$\varepsilon = 0.1, \quad a = 2, \quad (51)$$

which implies weak saturation of the gain in comparison with absorption, while the gain and SOC strengths, g and β , may be varied as physically relevant parameters controlling modes generated by the system.

Note that the nonlinearity in Eqs. (48) and (49) is entirely dissipative, as the equations do not include SPM or XPM terms. The domination of the dissipative terms over the conservative nonlinearity is the situation which is possible in laser cavities.

The objective is to construct solutions of Eqs. (48) and (49) in the form of 2D solitons morphed as a bound state of two components with vorticities $m - 1$ and $m + 1$, to comply with the condition that, due to the SOC acting through the second spatial derivatives in these equations, the difference between the components' vorticities must be $\Delta m = 2$. In polar coordinates (r, θ) , the relevant solutions with real chemical potential μ can be defined as

$$\psi_+ = \phi_+(r) \exp[-i\mu t + i(m - 1)\theta], \quad \psi_- = \phi_-(r) \exp[-i\mu t + i(m + 1)\theta], \quad (52)$$

with complex amplitude functions $\phi_{\pm}(r)$ satisfying the radial equations:

$$\mu\phi_+ = - \left[\frac{d^2}{dr^2} + \frac{1}{r} \frac{d}{dr} - \frac{1}{r^2} (m - 1)^2 \right] \phi_+ + if\phi_- + \beta \left(\frac{d^2}{dr^2} + \frac{2m + 1}{r} \frac{d}{dr} + \frac{m^2 - 1}{r^2} \right) \phi_-, \quad (53)$$

$$\mu\phi_- = - \left[\frac{d^2}{dr^2} + \frac{1}{r} \frac{d}{dr} - \frac{1}{r^2} (m + 1)^2 \right] \phi_- + if\phi_+ + \beta \left(\frac{d^2}{dr^2} - \frac{2m - 1}{r} \frac{d}{dr} + \frac{m^2 - 1}{r^2} \right) \phi_+, \quad (54)$$

where f is given by Eq. (50) with $|\psi_{\pm}|$ replaced by $|\phi_{\pm}|$.

The necessary condition of the stability of the zero solution of Eqs. (48) and (49) obviously amounts to condition

$$g < 1 + a. \quad (55)$$

On the other hand, a necessary condition for the ability of the saturable gain to maintain nontrivial modes is that the largest value of $f(n \equiv |\psi_+|^2 + |\psi_-|^2)$ in Eq. (50), which is attained at density

$$n_0 = \frac{\sqrt{a} - \sqrt{\varepsilon g}}{\sqrt{\varepsilon}(\sqrt{g} - \sqrt{\varepsilon a})}, \quad (56)$$

must be positive. The substitution of n_0 in Eq. (50) yields a lower bound for g , which, if combined with Eq. (55), defines the interval in which the gain coefficient may take its values:

$$\sqrt{\varepsilon a} + \sqrt{1 - \varepsilon} < g < 1 + a. \quad (57)$$

In particular, for values adopted in Eq. (51) interval (57) amounts to

$$1.396 < g < 3. \quad (58)$$

The b.c. for Eqs. (53) and (54) at $r \rightarrow 0$ is that ϕ_{\pm} must be vanishing as $r^{|m \mp 1|}$ at $r \rightarrow 0$, except for the case of $m \mp 1 = 0$, when the b.c. is $d\phi_{\pm}/dr|_{r=0} = 0$. At $r \rightarrow \infty$, soliton solutions must feature the exponential decay,

$$\phi_{\pm}(r) \sim r^{-1/2} \exp(-(\lambda_r + i\lambda_i)r), \quad (59)$$

with $\lambda_r > 0$.

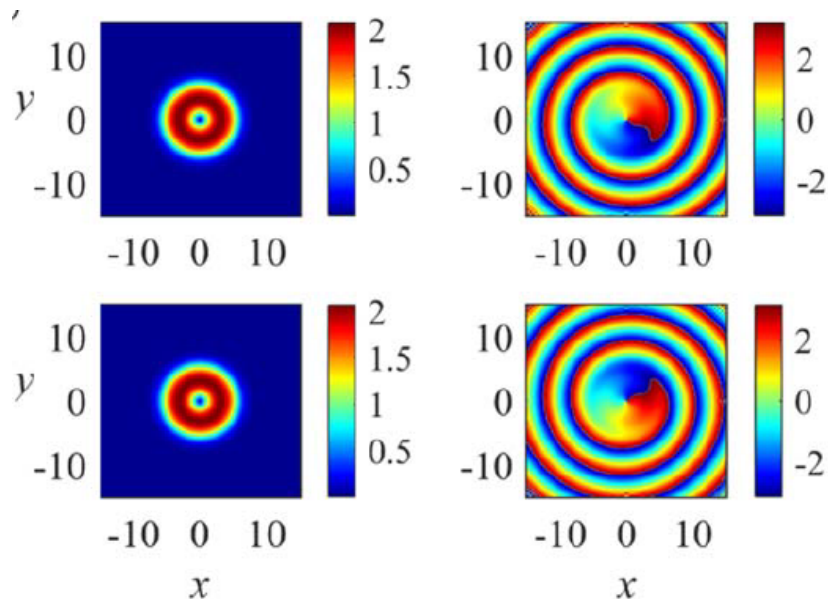


FIG. 36: Top views of amplitudes $|\psi_{\pm}(x, y)|$ and phases $\arg(\psi_{\pm}(x, y))$ of the two components of a stable VAV (vortex-antivortex) solution produced by Eqs. (53) and (54) with $\beta = 0.8$ and $g = 2.12$. Other parameters are fixed as per Eq. (51). The chemical potential of this VAV is $\mu = 0.072$ (source: Ref. [82]).

B. Results

There are two most essential species of soliton complexes produced by numerical solution of Eqs. (53) and (54) [82]. First, this is the vortex-antivortex (VAV) state, corresponding to $m = 0$ in Eq. (52). The name is due to the obvious fact that the components carry opposite vorticities, -1 and $+1$. The VAVs are similar to the HD (hidden-vorticity) states considered in two-component atomic BEC [88], cf. Eq. (5.26). The difference is that the incoherently coupled GP equations for the binary atomic BEC admit solutions with any combination of vorticities in the two components [89], while the vortex and antivortex components in VAV are inherently coupled by the SOC terms, which admits solely the difference $\Delta m = 2$ between the two components, as mentioned above

The second species is the SV (semi-vortex), corresponding to $m = 1$ in Eq. (5.52), with component vorticities 0 and 2. In SV solutions of the coupled Gross-Pitaevskii equations for the binary atomic BEC under the action of the SOC, SVs have two components with vorticities $(0, 1)$ or $(-1, 0)$, due to the fact that the SOC is represented in those equations by the first-order spatial derivatives mixing the components, hence the corresponding SVs must have $\Delta m = 1$ [76].

Examples of numerically found stable VAV and stable SV are displayed, respectively, in Figs. 36 and 37. Their stability was identified by means of calculation of eigenvalues for small perturbations added to the stationary solutions, and verified by direct simulations of the perturbed evolution.

The stability chart of the VAVs in the plane of control parameters (g, β) , which represent the gain and SOC strength in Eqs. (48), (49) and (50), while the saturation and loss parameters are fixed as per Eq. (51), is displayed in Fig. 38. The stability area as a whole lies within interval (57). Naturally, the blowup and decay occur if the gain is too large or too small, as indicated in the figure.

Note that the stability region for the VAV does not vanish at $\beta = 0$ (in the absence of SOC). In this limit, Eqs. (48) and (49) decouple into the single-component CGL equations, in which the vortex (or antivortex) DSs are not subject to the usual splitting instability because these equations do not contain self-focusing terms (conservative nonlinearity). If the latter terms are included, the VAVs become stable above a certain minimum value of the SOC strength, $\beta > \beta_{\min}$ [90].

Unlike the VAVs, the stability area of SVs is very narrow, therefore this soliton species is a less significant one in the present context. It was demonstrated that the stability of SVs can be enhanced by adding the Zeeman splitting to the system [90]. In terms of Eqs. (48) and (49), it means including terms $\mp \Omega \psi_{\pm}$ on the right-hand side of the equations, where Ω is the strength of the Zeeman splitting. Lastly, the system (without the Zeeman effect) may also sustain stable solutions in the form of MMs (mixed modes), which combine zero-vorticity terms and ones with vorticities ± 2 in both components [90].

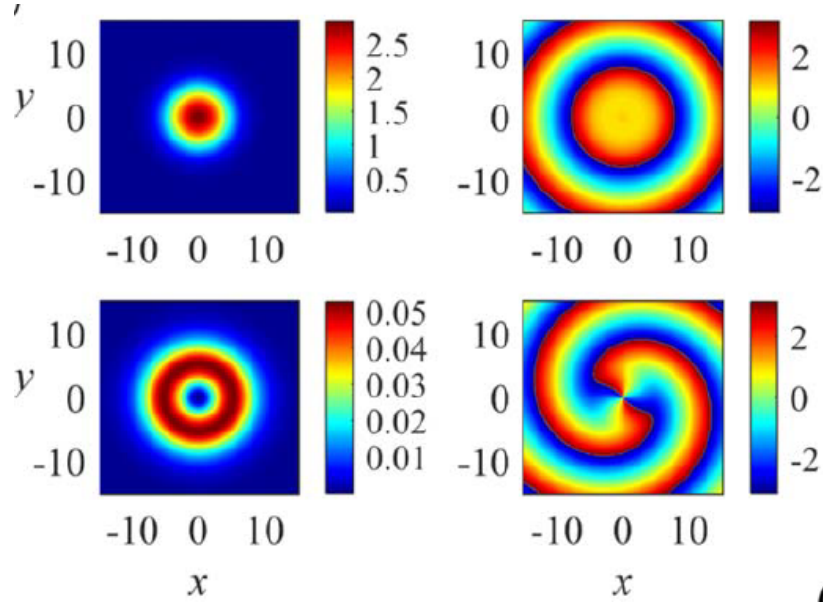


FIG. 37: The same as in Fig. 36, but for a stable SV (semi-vortex), with $\beta = 0.1$ and $g = 2.10$ (source: Ref. [82]).

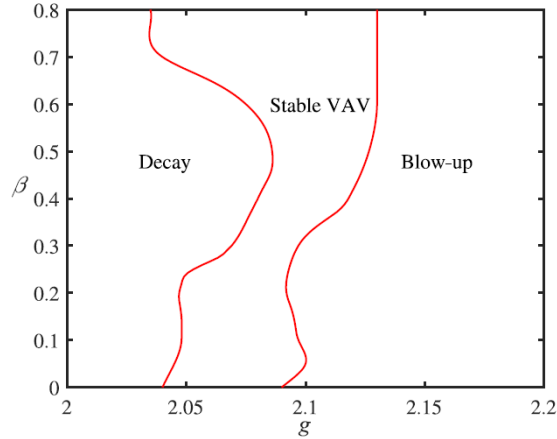


FIG. 38: Stability boundaries of the VAV solutions in the parameter plane (g, β) of the system of equations (48)-(50), while other parameters are fixed according to Eq. (51) (source: Ref. [82]).

IX. THREE-DIMENSIONAL DISSIPATIVE SOLITONS

A. 3D solitons in the free space

A natural 3D extension of the CGL equation (2), written in terms of the spatiotemporal right propagation in optics, includes the temporal GVD and spectral filtering (the imaginary part of GVD), with the respective coefficients $D \gtrless 0$ and $\gamma \geq 0$:

$$\left(\frac{\partial}{\partial z} + \delta\right)U = \left(\beta + \frac{i}{2}\right)\left(\frac{\partial^2}{\partial x^2} + \frac{\partial^2}{\partial y^2}\right)U + \left(\gamma + \frac{i}{2}D\right)U_{tt} + (\varepsilon + i)|U|^2U - (\mu + i\nu)|U|^4U. \quad (60)$$

Recall that $D > 0$ and $D < 0$ in Eq. (60) correspond to the anomalous and normal GVD, respectively, the former case being favorable for the creation of temporal solitons. As shown below, in the presence of the spectral filtering, $\beta > 0$, Eq. (60) generates stable 3D solitons for both $D > 0$ and $D < 0$ (creation of bright temporal solitons in setups with normal GVD is a problem of considerable interest in nonlinear optics [91, 92]). Further, it is assumed that the cubic and quintic conservative terms in Eq. (60) represent self-focusing (with the respective coefficient scaled

to be 1) and defocusing (accounted for by $\nu > 0$), respectively. Stationary solutions to Eq. (60), with propagation constant k and integer vorticity (winding number) S , are looked for, in the cylindrical coordinates (r, θ, z, t) , according to the general ansatz,

$$U(r, \theta, z, t) = \exp(ikz + iS\theta) \psi_S(r, t), \quad (61)$$

where complex function ψ_S satisfies equation

$$(ik + \delta) \psi_S = \left(\beta + \frac{i}{2} \right) \left(\frac{\partial^2}{\partial r^2} + \frac{1}{r} \frac{\partial}{\partial r} - \frac{S}{r^2} \right) \psi_S + \left(\gamma + \frac{i}{2} D \right) \frac{\partial^2 \psi_S}{\partial t^2} + (\varepsilon + i) |\psi_S|^2 \psi_S - (\mu + i\nu) |\psi_S|^4 \psi_S. \quad (62)$$

Stationary states are characterized by their 3D norm, which has the meaning of the total soliton's energy, in terms of optics:

$$E = \int \int \int |U(x, y, t)|^2 dx dy dt = 2\pi \int_0^\infty r dr \int_{-\infty}^{+\infty} |\psi_S(r, t)|^2. \quad (63)$$

The solutions with $S \geq 1$ may be considered as three-dimensional VRs, alias *vortex tori*, or “donuts”.

Stable fundamental ($S = 0$) and vortex DS solutions to Eq. (60) were first reported in Ref. [27]. Then, essential results were added in Refs. [28] and [29]. It was found that fundamental 3D solitons, produced by Eq. (60), are always stable, while, similar to what is known about solutions of the two-dimensional CGL equation (2), vortex solitons with winding number $S \geq 1$ may only be stable, against spontaneous splitting, in the presence of the diffusion term, with $\beta > 0$. On the other hand, the action of the spectral filtering is not necessary for the stability, i.e., Eq. (60) with $\gamma = 0$ can generate stable 3D vortex solitons. For this reason, the results are displayed below for $\gamma = 0$.

A set of typical shapes of stable 3D solitons with $S = 0, 1, 2, 3$ are displayed in Fig. 39, by means of their radial cross sections in the plane of $t = 0$ (temporal midplane) and temporal cross sections along the line of $x = y = 0$ (the spatial axis). A full 3D view of a stable toroidal vortex soliton with $S = 3$ is given in Fig. 40, which demonstrates the stability of this soliton against small perturbations.

Families of fundamental and vortex 3D solitons are characterized by dependences of their energy, calculated as per Eq. (63), on control parameters of the model. In particular, curves $E(\varepsilon)$ are displayed, for $S = 0, 1, 2, 3$, in Fig. 41. As seen in this figures, the family of the fundamental 3D solitons (with $S = 0$) is stable in its entire existence region, while for vortex solitons, with $S = 1, 2, 3$, the stability region is narrower than the existence domain. Furthermore, as mentioned above, in the case of $\beta = 0$ (no diffusion term in Eq. (60)) vortex-soliton families exist, but are completely unstable (as well as in the 2D version of the CGL equation).

The results for the existence and stability of the solitons are summarized in Fig. 42, in the form of the respective charts plotted in the plane of the nonlinear loss and gain parameters, (μ, ε) . The stability was identified by means of numerical solution of the eigenvalue problem for small perturbations, and verified by direct simulations of the perturbed simulations [27–29]) (see, in particular, Fig. 40).

The findings presented above were obtained with $D = 1$ in Eq. (42), i.e., for the anomalous sign of the GVD term. The same CGL equation with $D < 0$, i.e., with normal GVD, is also able to produce stable 3D fundamental and vortex solitons. In particular, all the fundamental solitons, with $S = 0$, remain stable in this case. Because the combination of the cubic self-focusing with normal GVD gives rise to stable CW (flat) states, the temporal cross section of the solitons tends to be flatter in this case, as seen in Fig. 43.

A noteworthy finding is that the stability area for the vortex solitons with $S = 1$ produced by Eq. (60) with the normal GVD ($D < 0$), is somewhat *broader* than its counterpart for $D > 0$, as seen in Fig. 44, which compares $E(\varepsilon)$ curves for both cases. This fact is natural, as the normal sign of the GVD precludes the possibility of the modulational instability in the temporal direction.

Essential results for 3D vortex DSs have been produced by the work with complex models of the spatiotemporal dynamics in laser cavities. Stable sophisticated states produced this work with those models include complexes of bound 3D solitons which may emulate motion of a solid body [93, 94], knotted solitons [95], and ones with a tubular structure [96]. This topic was reviewed in Refs. [94] and [86].

B. Collisions between 3D vortex solitons

As stated above, the CGL equation (60) gives rise to stable vortex solitons only in the presence of the diffusion term with $\beta > 0$, hence the equation has no Galilean invariance in the spatial plane (x, y) . Nevertheless, the existence of stable vortex solitons in the absence of the spectral filtering, $\gamma = 0$, makes it possible to set the soliton in free motion in the longitudinal (temporal) direction. Thus, it is possible to simulate collisions between the 3D solitons

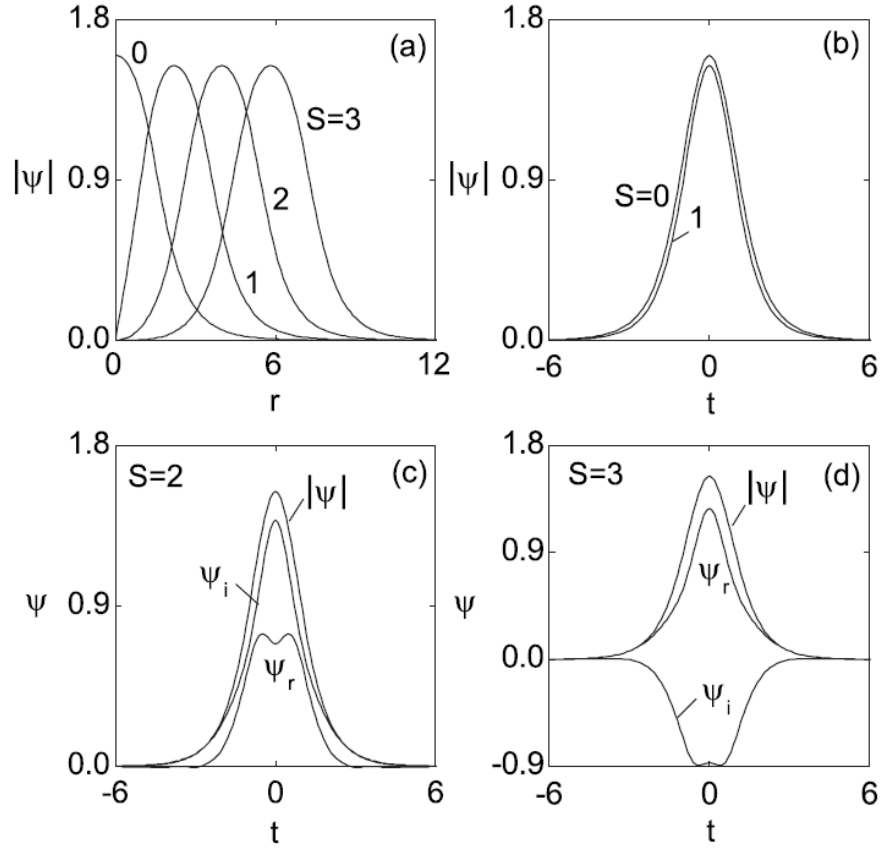


FIG. 39: (a) Profiles of the radial cross-section (at $t = 0$) of $|\psi_S(r, t)|$ in typical stable 3D dissipative solitons, with $S = 0, 1, 2, 3$, produced by numerical solution of Eq. (62). Panels (b)-(d): Cross sections of the absolute value and real and imaginary parts of $\psi_S(r, t)$ in the temporal direction (at $r = 0$). In (b), the temporal profiles for $S = 2$ and 3 completely overlap with that for $S = 1$. Parameters are $D = 1$, $\delta = 0.4$, $\beta = 0.5$, $\varepsilon = 2.2$, $\mu = 1$, $\nu = 0.1$, and $\gamma = 0$ (source: Ref. [29]).

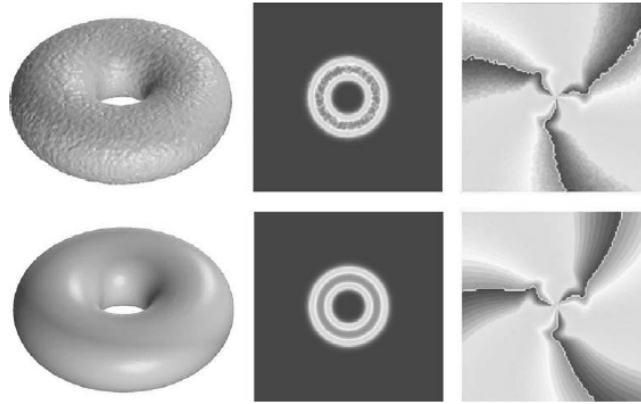


FIG. 40: Relaxation of an initially perturbed 3D vortex soliton with $S = 3$, produced by simulation of Eq. (60). The left and middle panels display the intensity distribution, $|U(x, y, t)|^2$, in the 3D form, and in the temporal mid plane, $t = 0$. The right panels: the phase distribution, $\arg(U(x, y))$, in the same plane. The top and bottom rows show, respectively, the input and the result of the evolution at $z = 800$. Parameters are $D = 1$, $\delta = 0.4$, $\beta = 0.5$, $\varepsilon = 2.3$, $\mu = 1$, $\nu = 0.1$, and $\gamma = 0$ (source: Ref. [29]).

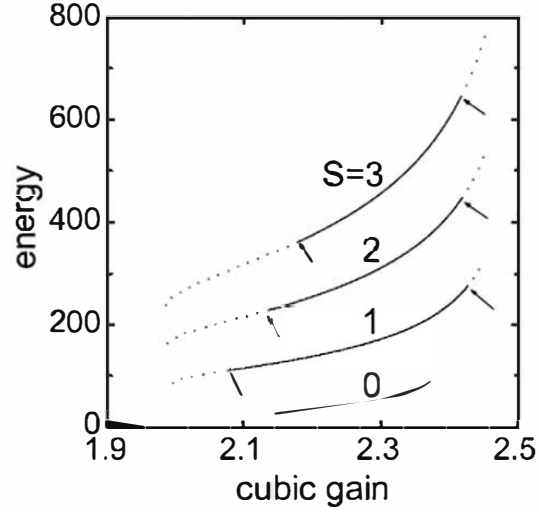


FIG. 41: Energy E of the 3D fundamental and vortical solitons with winding numbers S vs. the cubic-gain parameter ε . Other parameters in Eq. (60) are $D = 1$, $\delta = 0.4$, $\beta = 0.5$, $\mu = 1$, $\nu = 0.1$, and $\gamma = 0$. Dotted and solid segments correspond to unstable and stable solutions, respectively. Arrows indicate stability boundaries. The branch pertaining to $S = 0$ (fundamental solitons) is completely stable (source: Ref. [29]).

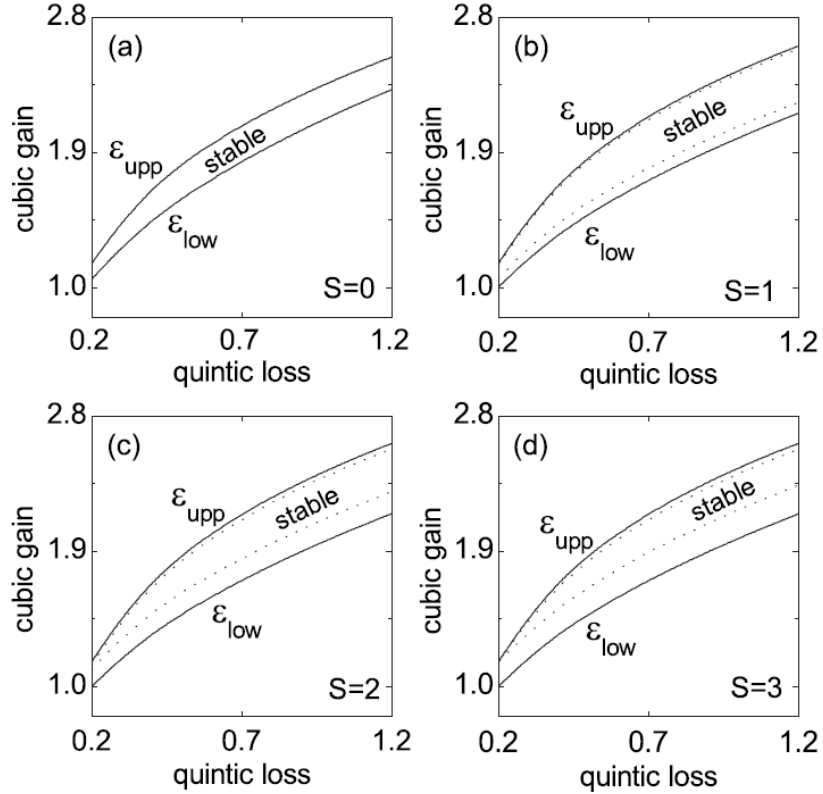


FIG. 42: The existence and stability domains of 3D solitons, with $S = 0, 1, 2, 3$, for $\beta = 0.5$, in the plane of the quintic-loss and cubic-gain coefficients, (μ, ε) , of Eq. (60). Other parameters are $D = 1$, $\delta = 0.4$, $\beta = 0.5$, $\gamma = 0$, and $\nu = 0.1$. The fundamental solitons ($S = 0$) exist and are stable between solid curves. The vortex solitons with $S = 1, 2, 3$ exist between solid curves and are stable between dotted ones, i.e., their stability domain is narrower than the existence range (source: Ref. [29]).

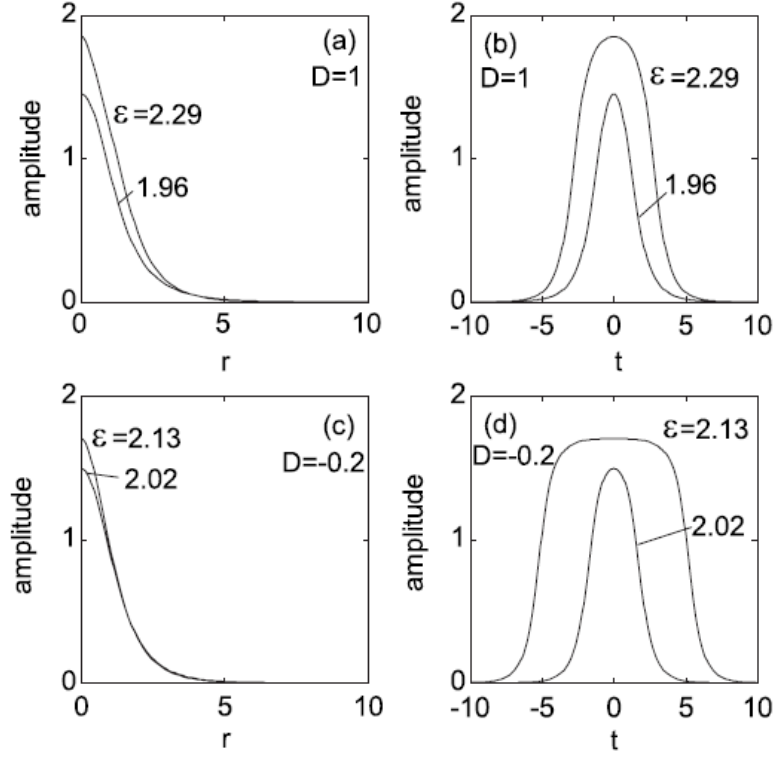


FIG. 43: (a,c) Profiles of the radial cross-section (at $t = 0$) of $|\psi_S(r, t)|$ in stable fundamental solitons, with $S = 0$, obtained as the numerical solution of Eq. (62). (b,d) Cross sections of $|\psi_S(r, t)|$ in the temporal direction (at $r = 0$) for the same solitons. Values of the GVD and cubic-gain coefficients, D and ϵ , are indicated in the panels. Note that panels (c) and (d) represent a stable fundamental soliton existing in the case of the *normal* GVD, with $D = -0.2 < 0$. Other parameters are $\delta = 0.4$, $\gamma = 0.5$, $\beta = 0$, $\mu = 1$, and $\nu = 0.1$ (source: Mihalache *et al.* (2007a)).

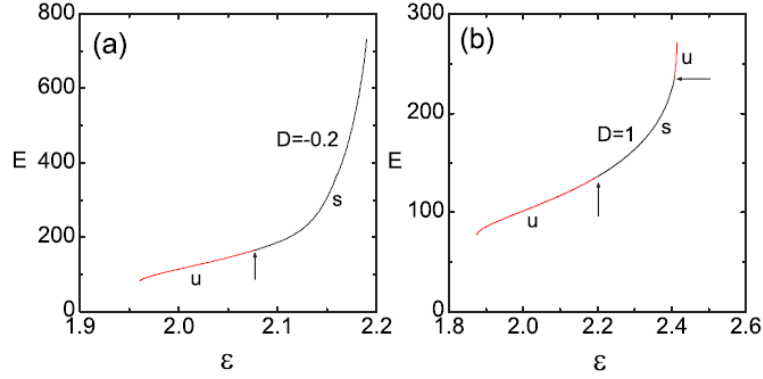


FIG. 44: The energy of the vortex solitons with $S = 1$ vs. the nonlinear-gain coefficient, ϵ . The solutions are produced by Eq. (60) with *normal* GVD, $D = -0.2$ in (a), and *anomalous* GVD, $D = 1$, in (b). Other parameters are $\delta = 0.4$, $\beta = 0.1$, $\gamma = 0.5$, $\mu = 1$, and $\nu = 0.1$. Stable (black) and unstable (red) portions of the solution branches are marked by symbols “s” and “u”, in addition to using the different colors in them. Arrows indicate stability boundaries (source: Mihalache *et al.* (2007a)).

(fundamental and vortical ones) moving along the longitudinal coordinate. Analysis of the collisions was developed using Eq. (60) with $\gamma = 0$ and $D = 1$ (the anomalous sign of the GVD term) [97–99]:

$$\left(\frac{\partial}{\partial z} + \delta\right)U = \left(\beta + \frac{i}{2}\right)\left(\frac{\partial^2}{\partial x^2} + \frac{\partial^2}{\partial y^2}\right)U + \frac{i}{2}U_{tt} + (\epsilon + i)|U|^2U - (\mu + i\nu)|U|^4U. \quad (64)$$

In the general form, simulations of collisions between 3D solitons is a challenging problem. However, it is quite tractable in the case of interactions between coaxial vortex solitons, which may collide moving in opposite directions

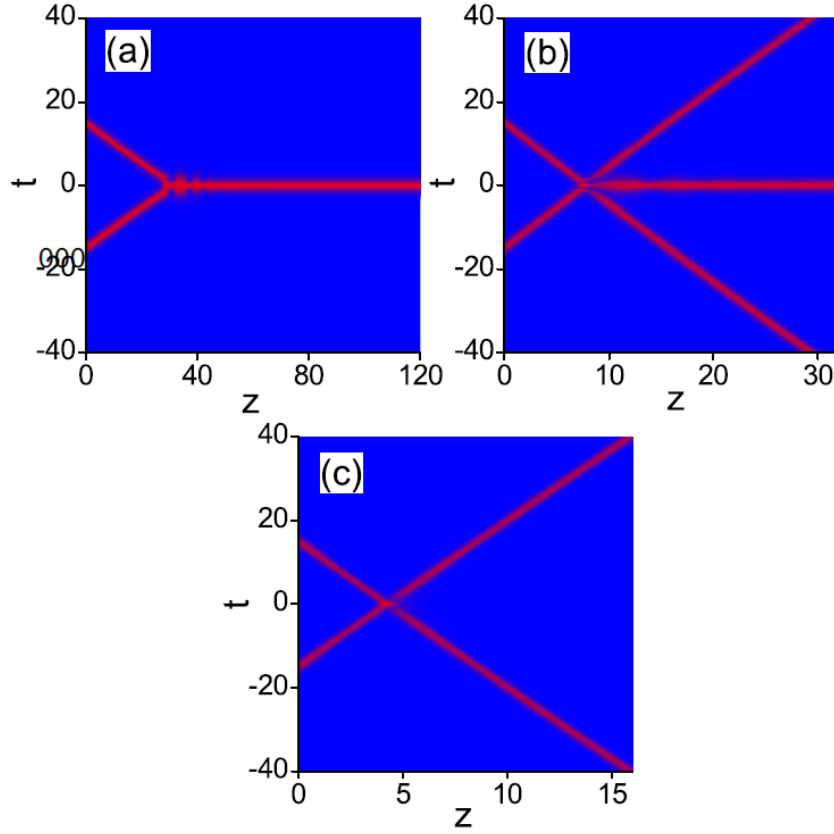


FIG. 45: Plots of $|U(x, y, t, z)|$ in the plane of $x = y = 0$ illustrate typical outcomes of collisions between two 3D dissipative vortex solitons with $S = 2$, produced by simulations of Eq. (5.64) with parameters (66) and initial conditions (65). (a) Merger of the slowly colliding solitons, which were set in motion by the kicks with $\chi = 0.5$ (see the detailed picture in Fig. 46). (b) Creation of an additional quiescent soliton with $S = 2$ in the case of $\chi = 2$. (c) Quasi-elastic collision of fast solitons in the case of $\chi = 4$, see the detailed picture in Fig. 47 (source: Ref. [97]).

along their common pivot. In particular, simulations of Eq. (60) for collisions between identical solitons, with equal vorticities, $S_1 = S_2$, and a large initial temporal separation, T , between them, were initiated by input

$$U_0(r, \theta, t) = \psi_S(r, t - T/2) \exp(iS\theta + i\chi t) + \psi_S(r, t + T/2) \exp(iS\theta - i\chi t), \quad (65)$$

where real $\pm\chi$ are initial kicks applied to the two solitons. Numerical results are displayed below in Figs. 45 – 47 for parameters

$$\delta = 0.4, \beta = 0.5, \varepsilon = 2.3, \mu = 1, \nu = 0.1. \quad (66)$$

For all values of the common vorticity, $S = 0, 1, 2$, the simulations of Eq. (64) with initial conditions (65) lead to the same qualitative results [97]: as shown in Fig. 45 for $S = 2$, slowly colliding solitons merge into a single one (which demonstrates gradually decaying intrinsic excitation), fast solitons quasi-elastically pass through each other, while at intermediate (moderately large) velocities the collision creates an additional soliton, with the same vorticity as carried by the original ones. The newly created soliton stays at the collision position.

The merger of slowly colliding solitons into a single one, and the generation of the additional soliton by those colliding at moderately large velocities, are illustrated in detail by Figs. 46 and 47, respectively. These pictures adequately represent generic outcomes of the inelastic collisions.

Collisions between a fundamental soliton and a vortex one, with $S = 1$ or 2 , were studied, by means of simulations of Eq. (64) [99]. Typical results are displayed, for the case of the vortex soliton with $S = 2$, in Fig. 48. The slow collision leads to merger of the solitons into a single one with $S = 0$, i.e., the vorticity is destroyed by the inelastic collision in this case, see Fig. 52(a). A faster collision produces, in Fig. 52(b), two separating solitons, both having $S = 0$, i.e., the vorticity is lost in this case too. Merger of the colliding solitons into a single one with $S = 0$ again occurs at somewhat larger value of the initial kick, as seen in Fig. 48(c). Finally, the fast collision seems quasi-elastic, but the

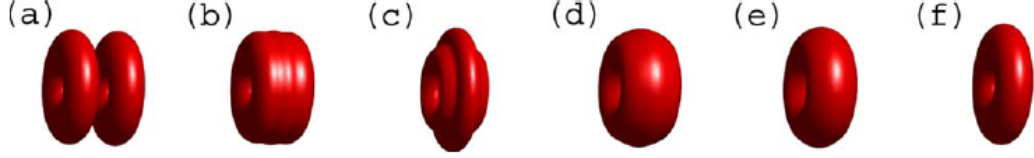


FIG. 46: Merger of the vortex solitons with winding numbers $S = 2$, which are set in motion as per initial conditions (65) with $\chi = 0.5$. Configurations are displayed at propagation distances $z = 25$ (a), 28 (b), 30 (c), 35 (d), 40 (e), and 60 (f). The figure corresponds to panel (a) in Fig. 45 (source: Ref. [97]).

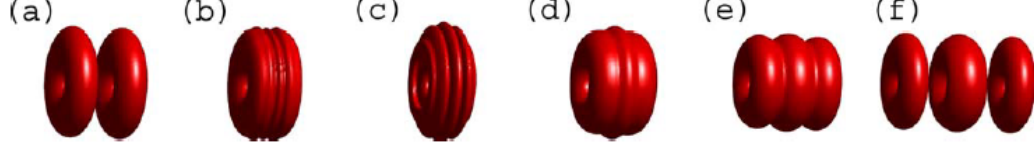


FIG. 47: The generation of an additional soliton with $S = 2$ by the collision of two vortex solitons (also with $S = 2$), which are set in motion as per initial conditions (65) with $\chi = 2$. Configurations are displayed at propagation distances $z = 3$ (a), 3.5 (b), 4 (c), 4.5 (d), 5 (e), and 5.5 (f). The figure corresponds to panel (b) in Fig. 45 (source: Ref. [97]).

perturbed vortex soliton eventually splits in two fragments, each having $S = 0$. The latter outcome is displayed in Fig. 48(d).

Different results are produced by collisions of “counter-rotating” vortex solitons, which are taken as pairs of identical ones with opposite intrinsic vorticities $S_1 = -S_2 = 1$ or $S_1 = -S_2 = 2$ [98]. In this case, simulations of Eq. (64) with coefficients (66) were initiated by input

$$U_0(r, \theta, t) = \psi_S(r, t - T/2) \exp(iS\theta + i\chi t) + \psi_{-S}(r, t + T/2) \exp(-iS\theta - i\chi t), \quad (67)$$

cf. Eq. (65). The simulations demonstrates that, in both cases of input (67) with the vorticity pairs

$$(S_1, S_2) = (+1, -1) \quad (68)$$

and

$$(S_1, S_2) = (+2, -2), \quad (69)$$

the collision may lead, essentially, to five different outcomes, depending on the magnitude of kick χ in the input. These outcomes are summarized, for inputs corresponding to Eqs. (67) and (68) or (69), in Figs. 49 and 50. In these figures, the inputs are represented by plots (a).

First, if χ takes small values, the collisions are strongly inelastic, leading to the merger of the colliding vortex and antivortex solitons into a single compound state, which is a non-rotating dipole cluster in Fig. 49(b), and a non-rotating quadrupole cluster in Fig. 50(b), which are built of two or four fundamental solitons, respectively. These clusters, as well as those observed in plots (c) and (d) of both figures, very slowly expand in the course of the subsequent evolution, i.e., they do not represent true bound states.

At larger values of χ , the colliding solitons pass through each other, but they do not keep the intact structure. Instead, as seen in Figs. 49(c) and 50(c), each vortex is converted into a cluster, consisting, respectively, of two or four fundamental solitons. In both cases corresponding to Eqs. (68) and (69), the emerging clusters exhibit slow counter-rotation, which is subject to deceleration under the action of the viscous force induced by the term $\sim \beta$ in Eq. (64).

Next, still larger values of χ lead to an inelastic collisions illustrated by plots (d) in Figs. 49 and 50. In this case, there emerge a pair of slowly counter-rotating two-humped (in Fig. 49(d)) or four-humped (in 50(d)) localized states. In addition, the collision creates a single nonrotating dipole cluster (in Fig. 49(d)), or a quadrupole one (in 50(d)). In the course of the subsequent evolution, both two- and four-humped states slowly split into pairs of fundamental solitons.

Further increase of the initial kick χ in Eq. (67) leads, in Figs. 49(e) and 50(e), to the formation of the pairs of the counter-rotating two- or four-humped states, without the central cluster (unlike plots (d)). Lastly, at largest values of χ , the collision is, naturally, quasi-elastic, featuring the vortex and antivortex solitons passing through each other. The latter outcome is shown in Figs. 49(f) and 50(f).

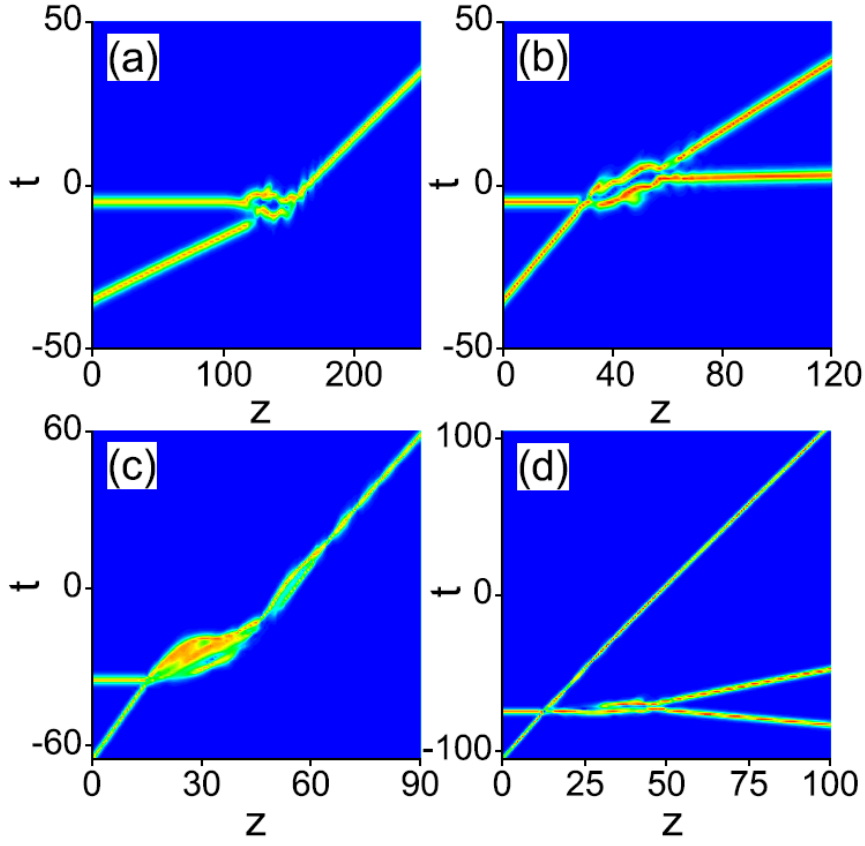


FIG. 48: Contour plots of $|U(z, t)|$ in the plane of $(x = y = 0)$, which illustrate outcomes of collisions of an initially kicked fundamental soliton ($S = 0$) and a quiescent (unkicked) stable one with $S = 2$. The results are produced by simulations of Eq. (64) with parameters $\delta = 0.4$, $\beta = 0.5$, $\varepsilon = 2.3$, $\mu = 1$, $\nu = 0.1$. In this case, the unperturbed solitons are found with propagation constants $k(S = 0) \approx 0.443$, $k(S = 1) \approx 0.500$, $k(S = 2) \approx 0.504$. The fundamental soliton is initially set in motion by kick $\chi = 0.2$ (a), 1 (b), 2 (c), and 2.5 (d), as in Eq. (65) (source: Ref. [99]).

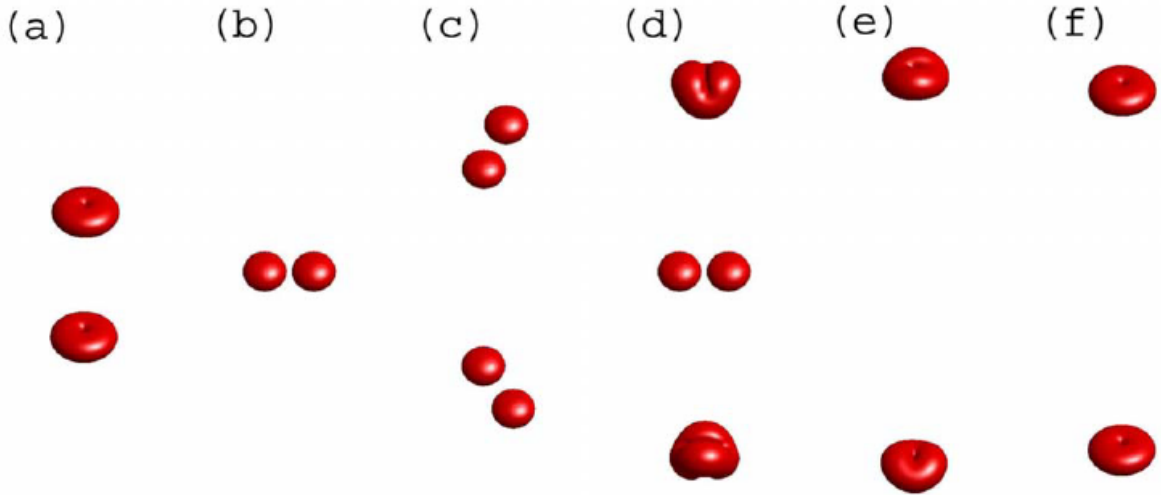


FIG. 49: A summary of outcomes of collisions between coaxial counter-rotating vortex solitons with $(S_1, S_2) = (+1, -1)$, produced by input (67). Plot (a) represents the input. The results, produced by simulations of Eq. (64), are shown in plots (c)-(f), which correspond to increasing values of kick χ in Eq. (67) (source: Ref. [98]).

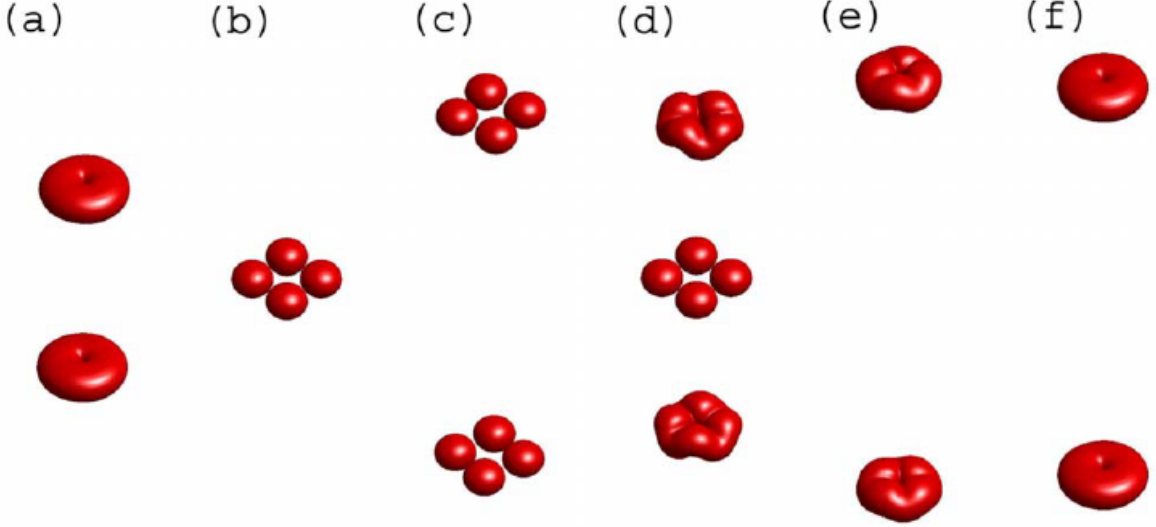


FIG. 50: The same as in Fig. 45, but for the input corresponding to Eqs. (67) and (69) (source: Ref. [98]).

C. Quasi-stable 3D vortex solitons supported by 2D potential lattices or a trapping potential

While the 3D CGL equation (60) cannot maintain stable vortex solitons in the absence of the diffusion term ($\beta = 0$), vorticity-carrying complexes with a four-peak structure can be made nearly stable, in the case of $\beta = 0$, with the help of the 2D potential lattice [100]. This is a significant finding because, as said above, the diffusion term does not appear in CGL models of laser systems, while the transverse spatially periodic structure is present if the system is based on the photonic crystal.

The corresponding model is similar to CGL equation (64) with $\beta = 0$, to which the lattice potential with scaled spatial period $L = \pi$ and depth $4V_0 > 0$ is added:

$$\left(\frac{\partial}{\partial z} + \delta\right)U = \frac{i}{2} \left(\frac{\partial^2}{\partial x^2} + \frac{\partial^2}{\partial y^2} + \frac{\partial^2}{\partial t^2}\right)U + (\varepsilon + i)|U|^2U - (\mu + i\nu)|U|^4U + iV_0[\cos(2x) + \cos(2y)]U. \quad (70)$$

Numerical solution of Eq. (70) give rise to the OS-centered (rhombic) four-peak complexes with vorticity $S = 1$, see typical examples in Fig. 51. Such solutions are stable against perturbations in the (x, y) plane, but slightly unstable against spontaneous separation of the constituents in the free longitudinal (temporal) direction. Nevertheless, for $V_0 = 4$, the separation instability of the vortex complex displayed in panels (c) of Fig. 51 is extremely weak, making it a practically stable state.

In the absence of the diffusivity, i.e., $\beta = 0$ in Eq. (60), 3D dissipative spatiotemporal solitons with embedded vorticity may be stabilized by the HO trapping potential, applied in the transverse plane (x, y) . The respective modification of Eq. (70) is [101]

$$\left(\frac{\partial}{\partial z} + \delta\right)U = \frac{i}{2} \left(\frac{\partial^2}{\partial x^2} + \frac{\partial^2}{\partial y^2} + \frac{\partial^2}{\partial t^2}\right)U + (\varepsilon + i)|U|^2U - \mu|U|^4U - i(x^2 + y^2)U. \quad (71)$$

Numerical solution of this equation has produced results which are similar to those outlined above in the connection to Eq. (60), where the stabilization of vortex DSs is provided by the diffusion term. Namely, a part of the family of 3D localized solutions with vorticity $S = 1$, generated by Eq. (71), are stable. A difference from the model based on Eq. (60) is that all solitons with $S \geq 2$ are unstable against splitting (recall that Eq. (60) produces stable vortex solitons with $S = 2$ and 3). Because of the presence of the trapping potential in Eq. (71), a soliton with $S = 2$ splits into a pair of vortex solitons with $S = 1$, which form a rotating bound state, as shown in Fig. 52.

X. CONCLUSION

As said in the Introduction, this review does not aim to cover all essential aspects of the work on dissipative multidimensional solitons. In particular, in addition to collisions between DSs, which are considered above in some

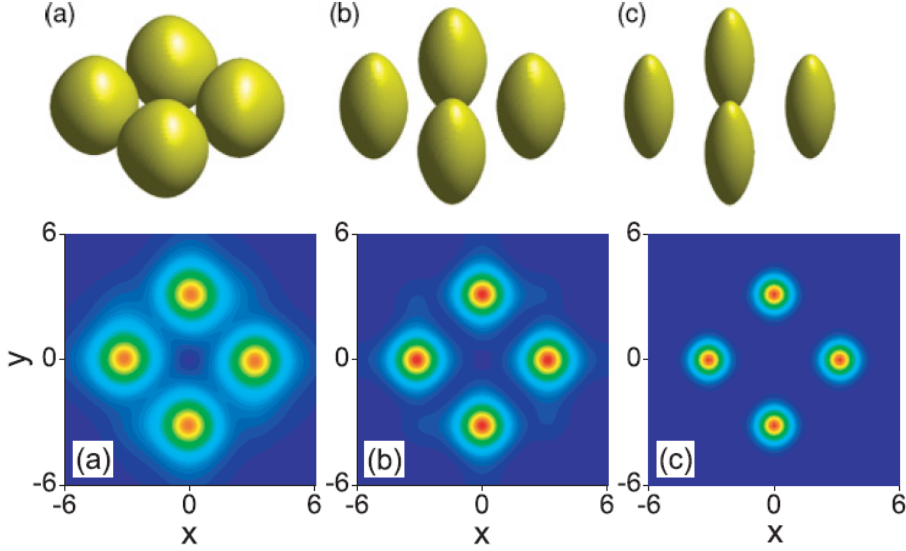


FIG. 51: The top and bottom plots are the 3D images and 2D cross sections in the plane of (x, y) of the four-peak complexes with winding number $S = 1$, produced as solutions of Eq. (70) with parameters $\delta = 0.4$, $\mu = 1$, and $\nu = 0.1$. The cubic-gain coefficient and strength of the lattice potential are $\varepsilon = 1.9$, $V_0 = 0.25$ in (a), $\varepsilon = 1.7$, $V_0 = 1$, and $\varepsilon = 1.8$, $V_0 = 4$ (source: Ref. [100]).

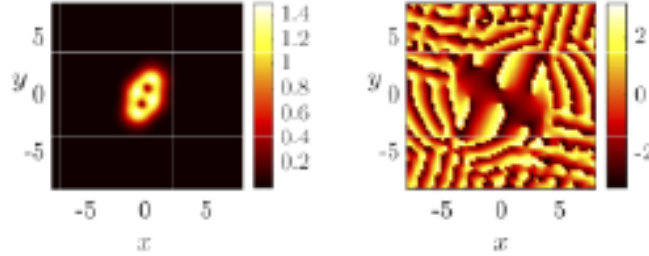


FIG. 52: The left and right panels display the snapshots of amplitude and phase, $|U(x, y)|$ and $\arg(U(x, y))$, in the temporal midplane, $t = 0$, of the rotating pair of vortex solitons with $S = 1$, produced by splitting of an unstable one with $S = 2$. The results are produced by simulations of Eq. (71) with $\delta = 0.1$, $\varepsilon = 0.6$, and $\mu = 0.4$ (source: Ref. [101]).

form, it may be interesting to consider stationary bound states of spatially separated 2D and 3D solitons, alias “soliton molecules”. Excited states of such “molecules”, in the form of oscillating bound states, may be quite interesting objects too. A theoretical tool for the prediction of potentially stable bound states of multidimensional DSs is offered by the analysis of an effective potential of interaction between far separated solitons [102]. Experimentally, such bound states were created only in effectively 1D setups, *viz.*, as coupled pairs of temporal solitons in fiber lasers [103–105].

A new branch of studies of light propagation in complex media represents topological photonics, which aims to create sophisticated optical patterns carrying robust intrinsic structures, which are characterized by the respective topological numbers. In particular, much interest has been recently drawn to emulation of topological insulators in photonics [106]. In most cases, such patterns were studied in the framework of linear optics. Solitons were addressed too, in the context of nonlinear topological photonics, although chiefly in the 1D form, such as edge solitons [107]. First results for 2D topological photonic solitons were reported recently [108, 109]. In the context of the present review, a challenging possibility may be to consider 2D topological solitons in artificially built nonlinear media, where losses are inevitable, hence they should be compensated by gain in an appropriate form.

Another area of photonics which is relevant in the present context is the study of self-trapped soliton-like states in exciton-polariton condensates filling semiconductor microcavities. Most works on this topic addressed 1D settings, but the consideration of 2D localized exciton-polariton states is relevant too [110]. The exciton-polariton condensates are essentially dissipative nonlinear media, in which losses are balanced by an external pump. In particular, vortex states

were created in such condensates experimentally [111, 112]. Spatially-periodic (lattice) potentials, which provide a major technique for the creation and stabilization of various soliton-like states (as discussed, in various contexts, in this review), are also available for the experimental work with the exciton-polariton condensates [113]. In particular, the lattice potential was used for the creation of 2D gap solitons in the exciton-polariton system, making use of the repulsive nonlinearity induced by dipole-dipole interactions between polarized excitons [114].

A different species of dissipative nonlinear systems in which losses are compensated by an external pump is represented by the Lugiato-Lefever (LL) equation [115]. Laser cavities offer an important physical realization of this model. Although in most works it was considered in the 1D form, the consideration of the 2D LL equation is relevant too, which suggests a possibility to look for 2D soliton-like states in this context [116–118]. Additional possibilities for the creation of localized states are offered by the 2D LL equation with a tightly localized (focused) pump term [119].

Finally, it is relevant to mention that theoretical analysis was also developed for various types of 2D solitons in \mathcal{PT} -symmetric systems, with the cubic or CQ nonlinearity and a complex potential, composed of spatially even real and odd imaginary parts [120–126]. As mentioned above, although the \mathcal{PT} -symmetric systems may be considered as a very special case of dissipative settings, they give rise not to isolated solitons, but to their continuous families (like in conservative models), up to the \mathcal{PT} -symmetry-breaking point. In the theoretical works on 2D \mathcal{PT} -symmetric solitons, including ones with embedded vorticity, stability is a crucially important issue.

Acknowledgments

I would like to thank Profs. Marcel Clerc, Karin Alfaro-Bittner, Alejandro Leon, Rene Rojas, and Mustapha Tlidi, the Guest Editors of the special issue of Chaos, Solitons & Fractals on the topic of *New trends on instabilities and nonequilibrium structures*, for their invitation to submit a contribution for this special issue. The work was supported, in part, by the Israel Science foundation through grant No. 1286/17.

-
- [1] M. C. Cross and P. C. Hohenberg, Pattern formation outside of equilibrium, *Rev. Mod. Phys.* **65**, 851-1124 (1993).
 - [2] Rosanov N. N., *Spatial hysteresis and optical patterns* (Springer: Berlin, 2002).
 - [3] R. Hoyle, *Pattern Formation: An introduction to methods* (Cambridge University Press: Cambridge, 2006).
 - [4] I. S. Aranson and L. Kramer, The world of the complex Ginzburg-Landau equation, *Rev. Mod. Phys.* **74**, 99-143 (2002).
 - [5] B. A. Malomed, Complex Ginzburg-Landau equation, in *Encyclopedia of Nonlinear Science*, pp. 157-160, editor A. Scott (Routledge: New York, 2005).
 - [6] B. A. Malomed, Evolution of nonsoliton and “quasiclassical” wavetrains in nonlinear Schrödinger and Korteweg - de Vries equations with dissipative perturbations, *Physica D* **29**, 155-172 (1987).
 - [7] O. Descalzi, M. Argentina, and E. Tirapegui, Stationary localized solutions in the subcritical complex Ginzburg-Landau equation, *Int. J. Bif. Chaos* **12**, 2459-2465 (2002).
 - [8] O. Descalzi, P. Gutierrez, and E. Tirapegui, Localized structures in nonequilibrium systems, *Int. J. Mod. Phys. C* **16**, 1909-1916 (2005).
 - [9] N. Akhmediev and A. Ankiewicz, editoris: *Dissipative Solitons: From Optics to Biology and Medicine* (Springer-Verlag: Berlin and Heidelberg, 2008).
 - [10] A. W. Liehr, *Dissipative Solitons in Reaction Diffusion Systems* (Springer-Verlag: Berlin and Heidelberg, 2008).
 - [11] D. Mihalache, Three-dimensional dissipative optical solitons, *Cent. Eur. J. Phys.* **6**, 582-587 (2008).
 - [12] O. Descalzi, M. Clerc, S. Residori, and G. Assanto, G. (Eds.). *Localized States in Physics: Solitons and Patterns* (Springer: Heidelberg, 2011).
 - [13] L. M. Hocking and K. Stewartson, On the nonlinear response of a marginally unstable plane parallel flow to a two-dimensional disturbance, *Proc. Royal Soc. London A* **326**, 289-313 (1972).
 - [14] N. R. Pereira and L. Stenflo, Nonlinear Schrödinger equation including growth and damping, *Phys. Fluids* **20**, 1733-1734 (1977).
 - [15] B. A. Malomed, (INVITED) Vortex solitons: Old results and new perspectives, *Physica D* **399**, 108-137 (2019).
 - [16] B. A. Malomed, D. Mihalache, F. Wise, and L. Torner, Spatiotemporal optical solitons, *J. Optics B: Quant. Semicl. Opt.* **7**, R53-R72 (2005).
 - [17] B. A. Malomed, D. Mihalache, F. Wise, and L. Torner, Viewpoint: On multidimensional solitons and their legacy in contemporary Atomic, Molecular and Optical physics, *J. Phys. B: At. Mol. Opt. Phys.* **49**, 170502 (2016).
 - [18] B. A. Malomed, Multidimensional solitons: Well-established results and novel findings, *Eur. Phys. J. Special Topics* **225**, 2507-2532 (2016).
 - [19] D. Mihalache, Multidimensional localized structures in optical and matter-wave media: A topical survey of recent literature, *Romanian Reports in Physics* **69**, 403 (2017).
 - [20] Y. Kartashov, G. Astrakharchik, B. Malomed, and L. Torner, Frontiers in multidimensional self-trapping of nonlinear fields and matter, *Nature Reviews Physics* **1**, 185-197 (2019).

- [21] S. Fauve and O. Thual, Subcritical instabilities in dissipative systems generate solitary waves, *Phys. Rev. Lett.* **64**, 282-284 (1990).
- [22] Y. S. Kivshar and G. P. Agrawal, *Optical Solitons: From Fibers to Photonic Crystals* (Academic Press, San Diego, 2003).
- [23] A. M. Sergeev A. M. and V. I. Petviashvili, Spiral solitons in active media with excitation threshold, *Dokl. AN SSSR* **276**, 1380-1384 (1984) [English translation: *Sov. Phys. Doklady* **29**, 493 (1984)].
- [24] L. Bergé, Wave collapse in physics: principles and applications to light and plasma waves, *Phys. Rep.* **303**, 259-370 (1998).
- [25] C. Sulem C. and P.-L. Sulem, *The Nonlinear Schrödinger Equation: Self-Focusing and Wave Collapse* (Springer, New York, 1999).
- [26] G. Fibich, *The Nonlinear Schrödinger Equation: Singular Solutions and Optical Collapse* (Springer, Heidelberg, 2015).
- [27] D. Mihalache D., D. Mazilu, F. Lederer, Y. V. Kartashov, L.-C. Crasovan, L. Torner, and B. A. Malomed, Stable vortex tori in the three-dimensional cubic-quintic Ginzburg-Landau equation, *Phys. Rev. Lett.* **97**, 073904 (2006).
- [28] D. Mihalache, D. Mazilu, F. Lederer, H. Leblond, B. A. Malomed, Stability of dissipative optical solitons in the three-dimensional cubic-quintic Ginzburg-Landau equation, *Phys. Rev. A* **75**, 033811 (2007a).
- [29] D. Mihalache, D. Mazilu, F. Lederer, H. Leblond, and B. A. Malomed, Stability limits for three-dimensional vortex solitons in the Ginzburg-Landau equation with the cubic-quintic nonlinearity, *Phys. Rev. A* **76**, 045803 (2007b).
- [30] H. A. Haus, Mode-locking of lasers, *IEEE J. Sel. Top. Quant. Electr.* **6**, 1173-1185 (2000).
- [31] U. Keller, Recent developments in compact ultrafast lasers, *Nature* **424**, 831-838 (2003).
- [32] Q. L. Bao, H. Zhang, Y. Wang, Z. H. Ni, Y. L. Yan, Z. X. Shen, K. P. Loh, and D. Y. Tang, Atomic-Layer graphene as a saturable absorber for ultrafast pulsed lasers, *Adv. Functional Materials* **19**, 3077-3083 (2009).
- [33] M. E. Fermann and I. Hartl, Ultrafast fiber laser technology, *IEEE J. Sel. Top. Quant. Electr.* **15**, 191-206 (2009).
- [34] T. Elsass, K. Gauthron, G. Beaudoin, I. Sagnes, R. Kuszelewicz, and S. Barbay, Control of cavity solitons and dynamical states in a monolithic vertical cavity laser with saturable absorber, *Eur. Phys. J. D* **59**, 91-96 (2010).
- [35] A. Y. Zykin, D. V. Skryabin, and Y. V. Kartashov, Topological solitons in arrays of mode-locked lasers, *Opt. Lett.* **46**, 2123-2126 (2021).
- [36] V. V. Konotop, J. Yang, and D. A. Zezyulin, Nonlinear waves in PT -symmetric systems, *Rev. Mod. Phys.* **88**, 035002 (2016).
- [37] M. G. Clerc, G. González-Cortés, and S. Echeverría-Alar, Localized dissipative vortices in chiral nematic liquid crystal cells, *Phys. Rev. Res.* **4**, L022021 (2022).
- [38] S. V. Suchkov, A. A. Sukhorukov, J. Huang, S. V. Dmitriev, C. Lee, and Y. S. Kivshar, Nonlinear switching and solitons in PT -symmetric photonic systems, *Laser Phot. Rev.* **10**, 177-213 (2016).
- [39] L.-C. Crasovan, B. A. Malomed, and D. Mihalache, Stable vortex solitons in the two-dimensional Ginzburg-Landau equation, *Phys. Rev. E* **63**, 016605 (2000).
- [40] P. Couillet P., L. Gil, and F. Rocca, Optical vortices, *Opt. Commun.* **73**, 403-408 (1989).
- [41] D. Mihalache, D. Mazilu, V. Skarka, B. A. Malomed, H. Leblond, N. B. Aleksić, and F. Lederer, Stable topological modes in two-dimensional Ginzburg-Landau models with trapping potentials. *Phys. Rev. A* **82**, 023813 (2010).
- [42] H. Leblond, B. A. Malomed, and D. Mihalache, Stable vortex solitons in the Ginzburg-Landau model of a two-dimensional lasing medium with a transverse grating, *Phys. Rev. A* **80**, 033835 (2009).
- [43] V. Skarka, N. B. Aleksić, H. Leblond, B. A. Malomed, and D. Mihalache, Varieties of stable vortical solitons in Ginzburg-Landau media with radially inhomogeneous losses, *Phys. Rev. Lett.* **105**, 213901 (2010).
- [44] V. E. Lobanov, Y. V. Kartashov, V. A. Vysloukh, and L. Torner, Stable radially symmetric and azimuthally modulated vortex solitons supported by localized gain, *Opt. Lett.* **36**, 85-87 (2011).
- [45] Y. V. Kartashov, V. V. Konotop, V. A. Vysloukh, and D. A. Zezyulin, Guided modes and symmetry breaking supported by localized gain, in *Spontaneous Symmetry Breaking, Self-Trapping, and Josephson Oscillations*, edited by B. A. Malomed, pp. 167-200 (Springer-Verlag: Berlin and Heidelberg, 2013).
- [46] L.-C. Crasovan, B. A. Malomed, and D. Mihalache, Erupting, flat-top, and composite spiral solitons in the two-dimensional Ginzburg-Landau equation, *Phys. Lett. A* **289**, 59-65 (2001).
- [47] B. N. Aleksić, N. B. Aleksić, V. Skarka, and M. Belić, Stability and nesting of dissipative vortex solitons with high vorticity, *Phys. Rev. A* **91**, 043832 (2015).
- [48] Z. Wu and Z. Wang, Optical vortices in the Ginzburg-Landau equation with cubic-quintic nonlinearity, *Nonlinear Dyn.* **94**, 2363-2371 (2018).
- [49] Soto-Crespo J. M., N. Akhmediev, and A. Ankiewicz, Pulsating, creeping, and erupting solitons in dissipative systems, *Phys. Rev. Lett.* **85**, 2937-2940 (2000).
- [50] H. Sakaguchi, Motion of pulses and vortices in the cubic-quintic complex Ginzburg-Landau equation without viscosity, *Physica D* **210**, 138-148 (2005).
- [51] B. A. Malomed and H. G. Winful, Stable solitons in two-component active systems, *Phys. Rev. E* **53**, 5365-5368 (1996).
- [52] B. A. Malomed, Solitary pulses in linearly coupled Ginzburg-Landau equations, *Chaos* **17**, 037117 (2007).
- [53] J. Atai and B. A. Malomed, Stability and interactions of solitons in two-component systems, *Phys. Rev. E* **54**, 4371-4374 (1996).
- [54] P. V. Paulau, D. Gomila, P. Colet, B. A. Malomed, and W. J. Firth, From one- to two-dimensional solitons in the Ginzburg-Landau model of lasers with frequency-selective feedback, *Phys. Rev. E* **84**, 036213 (2011).
- [55] P. V. Paulau, D. Gomila, P. Colet, N. A. Loiko, N. N. Rosanov, T. Ackemann, and W. J. Firth, Vortex solitons in lasers with feedback, *Opt. Express* **18**, 8859-8866 (2010).
- [56] Porrás M. A., A. Parola, D. Faccio, A. Dubietis, and P. Di Trapani, Nonlinear unbalanced Bessel beams: Stationary

conical waves

supported by nonlinear losses, *Phys. Rev. Lett.* **93**, 153902 (2004).

- [57] M. A. Porras and C. Ruiz-Jiménez, Nondiffracting and nonattenuating vortex light beams in media with nonlinear absorption of orbital angular momentum, *J. Opt. Soc. Am. B* **31**, 2657-2664 (2014).
- [58] Porras M. A., M. Carvalho, H. Leblond, and B. A. Malomed, Stabilization of vortex beams in Kerr media by nonlinear absorption, *Phys. Rev. A* **94**, 053810 (2016).
- [59] A. S. Desyatnikov, A. A. Sukhorukov, and Y. S. Kivshar, Azimuthons: Spatially modulated vortex solitons, *Phys. Rev. Lett.* **95**, 203904 (2005).
- [60] G. Y. Li, Azimuthons and pattern formation in annularly confined exciton-polariton Bose-Einstein condensates, *Phys. Rev. A* **93**, 013837 (2016).
- [61] C. Ruiz-Jimenez, H. Leblond, M. A. Porras, and B. A. Malomed, Rotating azimuthons in dissipative Kerr media excited by superpositions of Bessel beams, *Phys. Rev. A* **102**, 063502 (2020).
- [62] C. Ruiz-Jiménez, H. Leblond, M. A. Porras, and B. A. Malomed, Rotating azimuthons in dissipative Kerr media excited by superpositions of Bessel beams, *Phys. Rev. A* **102**, 063502 (2020).
- [63] V. Skarka, N. B. Aleksić, M. Lekić, B. N. Aleksić, B. A. Malomed, D. Mihalache, and H. Leblond, Formation of complex two-dimensional dissipative solitons via spontaneous symmetry breaking, *Phys. Rev. A* **90**, 023845 (2014).
- [64] V. E. Lobanov, A. A. Kalinovich, O. V. Borovkova, and B. A. Malomed, Fundamental and vortex dissipative quadratic solitons supported by spatially localized gain, *Phys. Rev. A* **105**, 013519 (2022).
- [65] V. L. Kalashnikov and S. Wabnitz, A “metaphorical” nonlinear multimode fiber laser approach to weakly dissipative Bose-Einstein condensates, *EPL* **133**, 34002 (2021).
- [66] T. Mayteevarunyoo, T., B. A. Malomed, and D. V. Skryabin, One- and two-dimensional modes in the complex Ginzburg-Landau equation with a trapping potential, *Opt. Exp.* **26**, 8849-8865 (2018).
- [67] R. Driben, B. A. Malomed, A. Gubeskys, and J. Zyss, Cubic-quintic solitons in the checkerboard potential, *Phys. Rev. E* **76**, 066604 (2007).
- [68] B. B. Baizakov, B. A. Malomed, and M. Salerno, Multidimensional solitons in periodic potentials, *Europhys. Lett.* **63**, 642-648 (2003).
- [69] V. Besse, H. Leblond, D. Mihalache, and B. A. Malomed, Pattern formation by kicked solitons in the two-dimensional Ginzburg-Landau medium with a transverse grating, *Phys. Rev. E* **87**, 012916 (2013).
- [70] B. B. Baizakov, B. A. Malomed, and M. Salerno, Multidimensional solitons in periodic potentials, *Europhys. Lett.* **63**, 642-648 (2003).
- [71] L. Yang J. and Z. H. Musslimani, Fundamental and vortex solitons in a two-dimensional optical lattice, *Opt. Lett.* **28**, 2094-2096 (2003).
- [72] E. A. Ostrovskaya and Y. S. Kivshar, Matter-wave gap vortices in optical lattices, *Phys. Rev. Lett.* **93**, 160405 (2004).
- [73] H. Sakaguchi and B. A. Malomed, Two-dimensional loosely and tightly bound solitons in optical lattices and inverted traps, *J. Phys. B* **37**, 2225-2239 (2004).
- [74] H. Sakaguchi and B. A. Malomed, Gap solitons in Ginzburg-Landau media, *Phys. Rev. E* **77**, 056606 (2008).
- [75] H. Sakaguchi H. and B. A. Malomed, Two-dimensional dissipative gap solitons, *Phys. Rev. E* **80**, 026606 (2009).
- [76] V. Galitski and I. B. Spielman, Spin-orbit coupling in quantum gases, *Nature* **494**, 49-54 (2013).
- [77] S. Schulz, S. Schumacher, and G. Czycholl, Spin-orbit coupling and crystal-field splitting in the electronic and optical properties of nitride quantum dots with a wurtzite crystal structure, *Eur. Phys. J. B* **64**, 51-60 (2008).
- [78] I. A. Shelykh, A. V. Kavokin, Y. G. Rubo, T. C. W. Liew, and G. Malpuech, Polariton polarization-sensitive phenomena in planar semiconductor microcavities, *Semicond. Sci. Technol.* **25**, 013001 (2010).
- [79] V. G. Sala, D. D. Solnyshkov, I. Carusotto, T. Jacqmin, I. Lemaître, H. Terças, A. Nalitov, M. Abbarchi, E. Galopin, I. Sagnes, J. Bloch, G. Malpuech, and A. Amo, Spin-Orbit coupling for photons and polaritons in microstructures, *Phys. Rev. X* **5**, 011034 (2015).
- [80] S. Dufferwiel, F. Li, E. Cancellieri, L. Giriunas, A. A. P. Trichet, D. M. Whittaker, P. M. Walker, F. Fras, E. Clarke, J. M. Smith, M. S. Skolnick, and D. N. Krizhanovskii, Spin textures of exciton-polaritons in a tunable microcavity with large TE-TM splitting, *Phys. Rev. Lett.* **115**, 246401 (2015).
- [81] O. Lafont, S. M. H. Luk, P. Lewandowski, N. H. Kwong, P. T. Leung, E. Galopin, A. Lemaître, J. Tignon, S. Schumacher, E. Baudin, and R. Binder, Controlling the optical spin Hall effect with light, *Appl. Phys. Lett.* **110**, 061108 (2017).
- [82] T. Mayteevarunyoo, B. Malomed, and D. Skryabin, Vortex modes supported by spin-orbit coupling in a laser with saturable absorption, *New J. Phys.* **20**, 113019 (2018).
- [83] P. Genevet, S. Barland, M. Giudici, and J. R. Tredicce, Bistable and addressable localized vortices in semiconductor lasers,” *Phys. Rev. Lett.* **104**, 223902 (2010).
- [84] M. Turconi, F. Prati, S. Barland, and G. Tissoni, Excitable solitons in a semiconductor laser with a saturable absorber, *Phys. Rev. A* **92**, 053855 (2015).
- [85] F. Gustave F., N. Radwell, C. McIntyre, J. P. Toomey, D. M. Kane, S. Barland, W. J. Firth, G.-L. Oppo, and T. Ackemann, Observation of mode-locked spatial laser solitons, *Phys. Rev. Lett.* **118**, 044102 (2017).
- [86] N. N. Rosanov, S. V. Fedorov, and N. A. Veretenov, Laser solitons in 1D, 2D and 3D, *Eur. Phys. J. D* **73**, 141 (2019).
- [87] H. Flayac, I. A. Shelykh, D. D. Solnyshkov, and G. Malpuech, Topological stability of the half-vortices in spinor exciton-polariton condensates, *Phys. Rev. B* **81**, 045318 (2010).
- [88] M. Brtko, A. Gammal, and B. A. Malomed, Hidden vorticity in binary Bose-Einstein condensates, *Phys. Rev. A* **82**, 053610 (2010).

- [89] T. Carmon, R. Uzdin, C. Pigier, Z. H. Musslimani, M. Segev, and A. Nepomnyashchy, Rotating propeller solitons, *Phys. Rev. Lett.* **87**, 143901 (2001).
- [90] H. Sakaguchi, B. A. Malomed, and D. V. Skryabin, Spin-orbit coupling and nonlinear modes of the polariton condensate in a harmonic trap, *New J. Phys.* **19**, 085003 (2017).
- [91] X. Wu, D. Y. Tang, H. Zhang, and L. M. Zhao, Dissipative soliton resonance in an all-normal-dispersion erbium-doped fiber laser, *Opt. Exp.* **17**, 5580-5584 (2009).
- [92] B. Oktem B., C. Ulgudur, and F. O. Ilday, Soliton-similariton fibre laser, *Nature Photonics* **4**, 307-311 (2010).
- [93] N. A. Veretenov, N. N. Rosanov, and S. V. Fedorov, Motion of complexes of 3D-laser solitons, *Opt. Quant., Electron.* **40**, 253-262 (2008).
- [94] N. N. Rosanov N. N., N. A. Veretenov, L. A. Nesterov, S. V. Fedorov, and A. N. Shatsev, Regular and stochastic motion of dissipative optical solitons, *JETP Lett.* **92**, 552-567 (2010).
- [95] N. Veretenov, S. Fedorov, and N. Rosanov, Topological vortex and knotted dissipative optical 3D solitons generated by 2D vortex solitons, *Phys. Rev. Lett.* **110**, 263901 (2017).
- [96] N. Veretenov, S. Fedorov, and N. Rosanov, Tubular laser solitons, *Opt. Lett.* **46**, 4076-4079 (2021).
- [97] D. Mihalache, D. Mazilu, F. Lederer, H. Leblond, and B. A. Malomed, Collisions between coaxial vortex solitons in the three-dimensional cubic-quintic complex Ginzburg-Landau equation, *Phys. Rev. A* **77**, 033817 (2008a).
- [98] D. Mihalache, D. Mazilu, F. Lederer, H. Leblond, and B. A. Malomed, Collisions between counter-rotating solitary vortices in the three-dimensional Ginzburg-Landau equation, *Phys. Rev. E* **78**, 056601 (2008b).
- [99] D. Mihalache, D. Mazilu, F. Lederer, H. Leblond, and B. A. Malomed, Collisions between spinning and nonspinning co-axial three-dimensional Ginzburg-Landau solitons, *Eur. Phys. J. Special Topics* **173**, 245-254 (2009).
- [100] D., Mihalache, D. Mazilu, F. Lederer, H. Leblond, and B. A. Malomed, Spatiotemporal solitons in the Ginzburg-Landau model with a two-dimensional transverse grating, *Phys. Rev. A* **81**, 025801 (2010a).
- [101] T. Maytevarunyo, B. A. Malomed, and D. V. Skryabin, Spatiotemporal dissipative solitons and vortices in a multi-transverse-mode fiber laser, *Opt. Exp.* **27**, 37364-37373 (2019).
- [102] B. A. Malomed. Potential of interaction between two- and three-dimensional solitons, *Phys. Rev. E* **58**, 7928-7933 (1998).
- [103] D. Tang, W. Man, H. Y. Tam, and P. Drummond, Observation of bound states of solitons in a passively mode-locked fiber laser, *Phys. Rev. A* **64**, 033814 (2001).
- [104] P. Grehu, F. Belhache, F. Gутty, and J.-M. Soto-Crespo, Phase-locked soliton pairs in a stretched-pulse fiber laser, *Opt. Lett.* **27**, 966-968 (2002).
- [105] S. Liu, Y. Cui, E. Karimi, and B. A. Malomed, On-demand harnessing of photonic soliton molecules, *Optica* **9**, 240-250 (2022).
- [106] M. Rechtsman, J. M. Zeuner, Y. Plotnik, Y. Lumer, D. Podolsky, F. Dreisow, S. Nolte, M. Segev, and A. Szameit, Photonic Floquet topological insulators, *Nature* **496**, 196-200 (2013).
- [107] D. Leykam and Y. D. Chong, Edge solitons in nonlinear-photonic topological Insulators, *Phys. Rev. Lett.* **117**, 143901 (2016).
- [108] M. A. Bandres, M. C. Rechtsman, and M. Segev, Topological photonic quasicrystals: fractal topological spectrum and protected transport, *Phys. Rev. X* **6**, 011016 (2016).
- [109] D. Smirnova, D. Leykam, Y. D. Chong, and Y. Kivshar, Nonlinear topological photonics, *Appl. Phys. Research* **7**, 021306 (2019).
- [110] H. Deng, H. Haug, and Y. Yamamoto, Exciton-polariton Bose-Einstein condensation, *Rev. Mod. Phys.* **82**, 1489-1537 (2010).
- [111] K. G. Lagoudakis, T. Ostatnický, A. V. Kavokin, Y. G. Rubo, R. Andre, and B. Deveaud-Pledran, Observation of half-quantum vortices in an exciton-polariton condensate, *Science* **326**, 974-976 (2009).
- [112] G. Roumpos, M. D. Fraser, A. Löffler, S. Hofling, A. Forchel, and Y. Yamamoto, Single vortex-antivortex pair in an exciton-polariton condensate, *Nature Phys.* **7**, 129-133 (2011).
- [113] Kim N. Y., K. Kusudo, C. J. Wu, N. Masumoto, A. Löffler, S. Hofling, N. Kumada, L. Worschech, A. Forchel, and Y. Yamamoto, Dynamical d-wave condensation of exciton-polaritons in a two-dimensional square-lattice potential, *Nature Phys.* **7**, 681-686 (2011).
- [114] E. A. Cerda-Méndez, D. Sarkar, D. N. Krizhanovskii, S. S. Gavrilov, K. Biermann, M. S. Skolnick, and P. V. Santos, Exciton-polariton gap solitons in two-dimensional lattices, *Phys. Rev. Lett.* **111**, 146401 (2013).
- [115] L. A. Lugiato and R. Lefever, Spatial dissipative structures in passive optical systems, *Phys. Rev. Lett.* **58**, 2209-2211 (1987).
- [116] C. J. de Valcarcel and K. Staliunas, Phase-bistable Kerr cavity solitons and patterns, *Phys. Rev. A* **87**, 043802 (2013).
- [117] M. Thidi and K. Panajotov, Two-dimensional dissipative rogue waves due to time-delayed feedback in cavity nonlinear optics, *Chaos* **27**, 013119 (2017).
- [118] C. Milian, Y. V. Kartashov, D. V. Skryabin, and L. Torner, Clusters of cavity solitons bounded by conical radiation, *Phys. Rev. Lett.* **121**, 103903 (2018).
- [119] W. B. Cardoso, L. Salasnich, and B. A. Malomed, Localized solutions of Lugiato-Lefever equations with focused pump, *Sci. Rep.* **7**, 16876 (2017).
- [120] Z. H. Musslimani, K. G. Makris, R. El-Ganainy, and D. N. Christodoulides, Optical solitons in \mathcal{PT} periodic potentials, *Phys. Rev. Lett.* **100**, 030402 (2008).
- [121] S. Nixon, L. J. Ge, and J. K. Yang, Stability analysis for solitons in \mathcal{PT} -symmetric optical lattices, *Phys. Rev. A* **85**, 023822 (2012).

- [122] *G. Burlak G. and B. A. Malomed, Stability boundary and collisions of two-dimensional solitons in \mathcal{PT} -symmetric couplers with the cubic-quintic nonlinearity, Phys. Rev. E **88**, 062904 (2013).*
- [123] *Z. Chen, J. Liu, S. Fu, Y. Li, and B. A. Malomed, Discrete solitons and vortices on two-dimensional lattices of \mathcal{PT} -symmetric couplers, Opt. Exp. **22**, 29679-29692 (2014).*
- [124] *J. K. Yang, Symmetry breaking of solitons in two-dimensional complex potentials, Phys. Rev. E **91**, 023201(2015).*
- [125] *E. Luz E., V. Lutsky, E. Granot, and B. A. Malomed, Robust \mathcal{PT} symmetry of two-dimensional fundamental and vortex solitons supported by spatially modulated nonlinearity”, Sci. Rep. **9**, 4483 (2019).*
- [126] *G.-M. Li, A. Li, S.-J. Su, Y. Zhao, K.-Y. Huang, G.-P. Zhou, L. Xue, and S.-L. Xu, Vector spatiotemporal solitons in cold atomic gases with linear and nonlinear \mathcal{PT} symmetric potentials, Opt. Exp. **29**, 14016-14024 (2021).*